Article:
Al- Sajed, O and Glover, P (2020) Dolomitisation, cementation and reservoir quality in three Jurassic and Cretaceous carbonate reservoirs in north-western Iraq. Marine and Petroleum Geology, 115. 104256. ISSN: 0264-8172

https://doi.org/10.1016/j.marpetgeo.2020.104256

Dolomitisation, cementation and reservoir quality in three Jurassic and Cretaceous carbonate reservoirs in north-western Iraq

Omar K. Mohammed Sajed[1] and Paul W.J.Glover[2]

[1]Department of Geology, College of Science, University of Mosul, Iraq, and School of Earth and Environment, University of Leeds, UK.

[2]School of Earth and Environment, University of Leeds, UK.

Abstract. Dolomitisation is a key diagenetic process, commonly improving reservoir quality in carbonate rocks. It is important in the Jurassic and Cretaceous carbonate reservoirs of north and north-western Iraq, creating primary and secondary pays in many oilfields (Kirkuk, Ain Zalah and Butmah). This paper addresses the impact of dolomitisation and cementation on the reservoir quality of three dolomitised carbonate formations (Butmah, Mauddud and Wajnah). Three different dolomitisation types were recognised: reflux dolomitisation, mixing zone, and burial dolomitisation. Extensive petrophysical measurements were carried out and have shown that differences in dolomite crystal size and cementation control the complexity of porosity, pore and pore throat size distributions, pore network connectivity, and permeability. Reflux dolomitisation exhibits widely spread porosities and permeabilities compared to the other two characterised dolomitisation models, indicating better reservoir properties wherever anhydrite cement is either absent or subsequently dissolved (as in the Butmah Formation). Mixing zone dolomitisation was encountered in the Mauddud and Wajnah formations, providing moderate to good reservoir properties, whereas burial dolomitisation generally provides poor to moderate reservoir properties in all three studied formations. It was noted that dolomite cementation provides poor reservoir properties in both the Butmah and Mauddud formations. Both the Mauddud and Wajnah formations show poroperm relationships with the degree of scatter dependent on both differences in crystal size and pore connectivity, indicating the degree of formation heterogeneity. Combined, both quantitative and qualitative observations indicate that dolomitisation cannot be considered in isolation, but is co-active and co-dependent upon dissolution, cementation and fracturing. All

of these processes can both cause and amplify dolomitisation, but can themselves be caused or amplified by dolomitisation. We have combined all of our observations to propose a new model which relates different reservoir quality outcomes to the occurrence, intensity and history of different diagenetic processes as a first step in the petrophysical quantification of the effect of diagenetic processes on reservoir quality.

Keywords. Dolomitisation; cementation; reservoir quality; heterogeneity; carbonate formations; diagenesis

1. Introduction

Dolomitisation is a geochemical process which affects the porosity and the morphology of the pore microstructure of carbonate rocks. It is considered to be one of a number of diagenetic processes which act upon the carbonate rock's primary matrix to ultimately define the carbonate formation's reservoir quality. Whereas much research has been carried out on diagenetic processes (Moore, 2001; Ahr, 2008; Tavakoli et al., 2011), we only have a qualitative understanding of how each of these processes affects reservoir quality. The quantification of each diagenetic process and its interactions with other processes in order that the effect of diagenesis on reservoir quality can be predicted is a goal which this paper partially addresses.

This paper contributes to that goal by studying the effect of dolomitisation and cementation on carbonate formations in northern Iraq. Numerous giant gas and condensate fields have been discovered in northern Iraq since the 1970s (Alsharhan and Nairn, 1997). Most of these fields produce from fractured and/or dolomitised formations.

Dolomitisation is defined as a diagenetic process where calcite ($CaCO_3$) is entirely or partly replaced by dolomite ($CaMg(CO_3)_2$) (Tucker, 1991). The replacement reduces the rock volume by about 12.3%, increasing the total porosity of the rock (North, 1985). Dolomitisation is characterised either as 'partial dolomitisation', when the dolomite replaces particular rock

components (grains or groundmass), or 'total dolomitisation', when the dolomite replaces all rock components (grains and groundmass) (Adams and Mackenzie, 1998).

Partial dolomitisation usually produces a mimetic texture due to the dolomitisation of the susceptible groundmass (aragonite or high Mg-calcite), leaving the stable mineralised grains which record the rock's primary fabric. Total dolomitisation produces non-mimetic textures from which the original fabric of the rock cannot be identified (Scholle and Ulmer-Scholle, 2003).

Dolomitisation can also be divided into early and late dolomitisation. Early dolomitisation is commonly constrained by occurrences of associated minerals (i.e., anhydrite, calcite) in the tidal flat environments, whereas late diagenetic dolomitisation increases the dolomite percent, thus increasing the porosity of the rocks when compaction and cementation processes are absent (Moore, 2001). Hydrothermal dolomitisation is a type of late dolomitisation that may occur in deeply buried rocks at high temperature and pressure, where highly saline brines create saddle dolomite textures in fractures and vuggy pores (Flugel, 2010). Hydrothermal dolomitisation, in general, increases the heterogeneity of carbonate rocks by forming cement or as a replacement that may occur from hydrothermal fluid advection, local redistribution of older dolomite during stylolitisation, and as a production of thermochemical sulphate reduction in semi-closed or closed systems (Machel, 2004).

Dolomitisation may reduce or increase the heterogeneity of carbonate rocks, consequently inducing heterogeneity in the rock's petrophysical properties (Ehrenberg and Nadeau, 2005; Ehrenberg, 2006; Lucia, 2007; Harris, 2010; Palermo et al., 2010; Ronchi et al., 2010; Rashid et al., 2015a; Rashid et al., 2015b). The improvement of reservoir properties by dolomitisation may be reduced by subsequent cementation and compaction or further improved by fracturing. Cementation also plays an important role in controlling the reservoir quality of dolomite units (Esrafili-Dizaji and Rahimpour-Bonab, 2009), where cementation as an early or late diagenesis may partly or totally occlude the pore network of the rock, reducing the pore connectivity and consequently reducing permeability and increasing electrical resistivity.

Three cement types were characterised in this study: anhydrite cement associated with reflux dolomitisation in the Butmah Formation, calcite cement filling some fractures, and dolomite cement (overdolomitisation or overgrowth dolomite cementation).

Generally, all rocks reduce in porosity and permeability as a function of depth aerial due to compaction. For depths of less than 2 km limestone and dolomitic limestone are more porous than dolostone. However, at greater depths dolostone becomes significantly more porous and permeable than limestone (Schmoker and Halley, 1982; Machel, 2004).

Fracturing influences the petrophysical properties of carbonate reservoirs when it either affects the primary matrix or a matrix which has already undergone diagenesis, giving access to fluids through an improved fracture network. The improved fluid flow may enhance access of fluids and improve reservoir quality, which then promotes further diagenesis, such as dolomitisation (Agosta et al., 2010; Larsen et al., 2010; Rashid, 2015a). Fractures are present to varying degrees in carbonate rocks and, if open, improve their fluid flow and reservoir quality and host economic mineral deposits or hydrocarbons. Fractures affect rocks to different degrees depending on their type, intensity and distribution within the rocks (Childs et al., 1997; Geraud et al., 2006; Hollis et al., 2017).

This paper reports the characterisation of the effect of dolomitisation type, intensity and history, as well as crystal size and cementation on the evolution of reservoir quality. These qualitative and quantitative observations have enabled us to develop a new model to describe the interactions between different types of diagenesis that are related to dolomitisation. This is the first step in our goal to develop a quantitative petrophysical approach to characterising the effect of all types of diagenesis on reservoir quality. The outcome of this study may be used in future to link with the depositional factors as the consideration of these factors requires access to samples from different dolomite formations relating to different depositional environments.

Such a study requires a large database of information culled from different methodologies. In this paper we use previously published work from other researchers (e.g., Rashid et al 2015a;

2015b; 2017; Hussein et al., 2017) to supplement almost 500 SEM slides studies of core material from three formations in three reservoirs, a wide range of petrophysical measurements, including porosity, permeability, nuclear magnetic resonance and capillary pressure measurements, on 43 core samples from the same formations and wells, as well as a wireline log analysis from the same wells. Nevertheless, we recognise that although sufficient to build a model for the effect of dolomitisation and its interactions with diagenetic processes, much more data is required to fully calibrate and validate the model.

2. Methods and materials

2.1 Lithofacies and stratigraphic units

The lithology was identified for the studied formation based on calibrating the identified lithological units from the core and cutting samples with the geophysical log responses.

Wireline log data were obtained from the North Oil Company (NOC) in Iraq. Digital copies of gamma ray, density, neutron, and sonic logs were collected from four wells (Bm-15, Az-16, Az-19 and Az-29) from the Butmah and Ain Zalah oilfields. The wireline well logs copies were digitised by Didger software (Version 3.5), then redrawn and analysed using Interactive Petrophysics software (Version 4.3) from Senergy Inc. To record or calculate precise values from the geophysical well logs, removing and/or editing unwanted signals was required. The three most common wireline log problems were corrected by depth shifting, applying environmental corrections and carrying out de-spiking and the removal of noise. The wireline log data have been combined with core descriptions from 3 wells (Bm-5, Az-16 and Az-19) in order to define lithofacies and describe the stratigraphic units of the studied formations.

Petrophysical analysis was carried out on core plug samples which are representative samples taken from the core intervals within the studied wells (Bm-15, Az-16, and Az-19). However, care was needed as there is a natural bias where core plugs from whole core are taken from well-indurated rock and fragile or fractured intervals are avoided. An effort was made to verify the core examination which included description of lithology, sedimentary

structures, macro porosity, fractures and oil show of the core intervals within the selected wells.

2.2 Porosity and permeability

The 64 core plug samples, 1.5 inches in diameter and 2.0 inches in length, were provided by the North Oil Company from the core intervals of the three formations within the studied wells. The core plug samples were cleaned using Soxhlet extraction (McPhee et al., 2015). The cleaned samples were dried in a temperature controlled oven at 60°C for 48 h. The porosity of the dried samples was obtained by helium pycnometry at a pressure ≤15 psig (Spain, 1992; McPhee et al., 2015) using the apparatus and protocols in the Wolfson laboratory at the University of Leeds. Porosity is calculated from the difference between the bulk and grain densities. The measurement was repeated three times for each core plug sample, with arithmetic mean values given in this paper.

Permeability was measured using a pulse-decay permeameter ($k \leq 1$ mD) (Jones, 1997; Jannot et al., 2007; Zhang et al., 2000; McPhee et al., 2015) using helium as a probe gas with confining pressure of 4500 psig. Using this technique the helium molecules flow is sufficient to enable that flow to be described by conventional fluid mechanical equations. When the gas pressure is low, there are few helium molecules per unit volume. Permeability measurements made at low gas pressures in small pores lead to an overestimation of the measured (or apparent) permeability. This is called the Klinkenberg effect (Tiab and Donaldson, 2012). The Klinkenberg correction was applied on the samples tested at effective stresses of 900 psig and at pore fluid pressure (750, 600, 450, and 300) psig respectively for all experimental measurements to correct for so-called gas 'slippage' when the requirement for continuity in the gas breaks down (Klinkenberg, 1941; Rushing et al., 2004; Haines et al., 2016).

2.3 Image analysis

A total of 456 thin-section slides were studied to describe the dolomite texture, crystal size and pore size, type and distribution. The samples were selected to cover the three studied

formations, especially the dolomitised units from wells Bm-15, Az-16, Az-19 and Az-29. All thin-section slides from cores and chippings were stained by a blue dye to highlight the pores in the thin section slide and using Dickson's (1965) staining technique (mixture staining technique using hydrochloric acid HCl, alizarin red ARS and potassium ferricyanide PF) to differentiate between such carbonate minerals as calcite, ferroan calcite, and dolomite.

Furthermore, scanning electron microscopy (SEM) has been used to provide images at the nanometric scale. High resolution quantitative measurements were made over selected areas of the sample by focusing the electron source on the sample surface and collecting secondary, backscatter and transmitted electron signals (Erdman and Bell, 2015). In this study, SEM was used on a total of 15 samples selected according to their dolomite texture and porosity and permeability relationship throughout the studied formations, each an approximate cuboid with a nominal side length of 7 mm, with broken and polished surfaces using magnifications of 1:500 to 1:10,000. The samples were cleaned using 1% acetic acid solvents to remove the volatile hydrocarbons and dust that might have affected the image quality. The samples were glued onto aluminium stubs and then coated with a conducting carbon film to be ready for digital recording of the SEM images. The captured images were analysed using ImageJ software to characterise pore and crystal sizes of the studied samples.

2.4 Carbon and oxygen isotope

Six samples in powder form were prepared by crushing 50 mg of sample material to a grain size of 200 mesh in an agate mortar for carbon and oxygen isotope analysis. These samples were dissolved in the pure phosphoric acid at a constant temperature of 25 °C for 72 h to measure the CO_2 emissions from the phosphate decomposition at 24 h later to 72 h. A thermo-finning MAT253 isotope-ratio mass spectrometer was used for the measurements. The oxygen-carbon isotopic composition of the samples was measured as δ and expressed in terms of the amount of ppt. The samples were calibrated against NBS-19 and LSVEC and isotopic data are reported against VPDB, with a 1δ standard error of 0.06‰ for C and 0.08‰ for O.

2.5 Mercury injection capillary pressure (MICP)

Mercury injection capillary pressure (MICP) tests using pressure up to 60,000 psig were carried out on 10 cleaned, evacuated samples that were chosen on the basis of their dolomite type, porosity, and permeability. The samples were cut to dimensions of 15 mm to 10 mm and the intrusion data were obtained using a Micro-meritics Autopore IV 9250 apparatus (Giesche, 2006). The raw MICP data were used to derive pore-throat size distributions (Jennings, 1987; Kopaska-Merkel and Amthor, 1988; Katz and Thompson, 1987; Glover et al., 2006) using the Young-Laplace equation (Washburn, 1921). The Glover and Dery (2010) method was used to obtain pore size distributions, and the Glover and Walker (2009) method was used to derive the crystal size distributions.

2.6 Electrical resistivity and cementation exponent

The core plug samples were saturated with a synthetic formation brine that was prepared based on the composition of the formation brine in the final well report of the studied wells. The formation brine was composed of 0.602 (gm/L) $Ca(HCO_3)_2$, 37.50 (gm/L) $CaCl_2$, 7.29 (gm/L) $MgCl_2$, and 94.982 (gm/L) NaCl. Full saturation was obtained by placing the core plugs in a vacuum desiccator, followed by saturation with the synthetic formation water for 24 hours. Subsequently, the samples were loaded into a high-pressure saturation core holder filled with the synthetic formation brine. The core holder was then left for 48 hours under a pressure of 100 psig. The brine and rock resistivity was then measured in order to calculate the formation factor for the selected samples. The resistivity of the formation brine was measured at laboratory temperature that was then converted to reservoir temperature using Arp's formula (Asquith and Krygowski, 2004). The formation factor was calculated straightforwardly from the electrical resistivity, and by using a simple equation to link the cementation exponent, formation factor and porosity, the cementation exponent for each sample could be calculated (Glover, 2015).

3. Geological setting and stratigraphy

This work considers three carbonate formations selected from the Ain Zalah and Butmah oilfields. The three formations are the Butmah Formation (Liassic/Lower Jurassic), the Mauddud Formation (Albian/Early Cretaceous), and the Wajnah Formation (Late Santonian/Late Cretaceous) (Jassim et al., 2006). Figure 1 shows the location of the Ain Zalah and Butmah oilfields with respect to the tectonic division of Iraq after Fouad, 2015.

The Ain Zalah oilfield is a structural trap, located in the Ain Zalah anticline about 60 Km north-west of Mosul city in northern Iraq. The Ain Zalah anticline, situated in the Zagros foothills zone (low folded zone) (Fouad, 2015), is about 20 km long by 5 km wide and has an elevation of 457m above sea level. Meanwhile, the Butmah anticline is located about 10 km south-east of and parallel to the Ain Zalah anticline in northern Iraq. It is an asymmetrical anticline consisting of two domes, eastern and western, and is about 12 km long and 6 km wide (Dunnington, 1958).

The Butmah Formation was deposited during the Liassic sequence (Lower Jurassic) of the late Permian-Liassic megasequence (AP6), according to Jassim et al. (2006), as shown in Figure 2. Tectonically, the study area suffered from extension at the northern and eastern margins of the Arabian plate in the Mid-Late Triassic which caused rifting followed by slow thermal subsidence in Norian-Liassic times. As a result, the Mesopotamian Basin post-rift infill was composed of uniform marginal marine clastics, evaporites and shallow lagoonal carbonates (Jasim and Goff, 2006; Aqrawi et al., 2010).

Figure 1. The location of the Butmah and Ain Zalah oilfields in north-western Iraq with the tectonic division of Iraq, after Fouad, 2015.

In this work, we used the term ‘lithofacies’ to identify the lithology of the studied formations, whereas ‘stratigraphic unit (unit)’ was used to characterise the vertical distribution of the lithofacies in succession. Consequently, the same lithofacies may be repeated two or three times with different stratigraphic unit numbers in succession.

The Butmah Formation in Well Bm-15 of the Butmah oilfield consists of five stratigraphic units which show three main lithofacies: (i) Lithofacies 1 is repeated three times in the Butmah Formation at Bm-15 as the stratigraphic units 1, 3, and 5. The lithofacies consist of microcrystalline limestone with or without anhydrite nodules. Fracturing effect was identified in the upper part of the stratigraphic units 1 and 3; (ii) Lithofacies 2 extends over a depth between 2544 and 2608 m (stratigraphic unit 2) as 17.8% of the total thickness of the Butmah Formation at well Bm-15 and is composed of dolomite interbedded with shale and some anhydrite nodules with fracturing effect on the middle and upper part of this unit; and (iii) Lithofacies 3 is the biggest lithofacies (stratigraphic unit 4), representing 53.4% of the gross thickness of the Butmah Formation at well Bm-15, and consists of dolomite that has anhydrite nodules and is interbedded in some intervals with anhydrite layers (Figure 3). The lower and upper contact of the Butmah Formation is concordant with marly limestone of the Baluti Formation and anhydrite beds of the Adaiyah formation respectively.

There is no outcrop of the Butmah Formation in Iraq, but it is penetrated by wells with a thickness of 162-500 m in north-western Iraq (Jasim et al., 2006). The thickness of the formation in the wells within the study area is constrained by Butmah-15 (402 m), and Ain Zalah-29 (473 m). The Butmah Formation graduates and interfingers horizontally to the Sarki Formation in north and north-eastern Iraq.

The Cretaceous succession is the most important sequence in Iraq due to the fact that the majority of the reservoir rocks belong to this succession. This stratigraphic sequence is represented by the Shiranish, Mushorah, Wajnah, Gir Bir, Mauddud, and Sarmord/Batiwah Formations at the Ain Zalah oilfield (Hart and Hay, 1974). According to Sharland et al. (2001), the Cretaceous succession includes two megasequences, AP8 and AP9, with a thickness of about 3000 m. The Late Tithonian-Early Turonian Megasequence (AP8) was deposited synchronously with new ocean floor spreading in the southern NeoTethys Ocean. This new phase of ocean floor spreading created a new passive margin along the north-eastern margin of the Arabian plate. The Late Turonian-Danian Megasequence (AP9) including the Mauddud

and Wajnah formations was deposited after the beginning of ophiolite obduction in the southern part of Neo-Tethys (Jasim and Buday, 2006).

The Mauddud Formation is equivalent to the Upper Qamchuqa and represents one of the most widespread Lower Cretaceous units in Iraq. The outcrop thickness of this formation is variable due to lateral facies changes and erosional truncation. In the subsurface, sections vary from 50-250 m in thickness (Jassim and Buday, 2006). The Mauddud Formation thickness in northern Iraq is reduced toward Mosul city, with a sharp increase in thickness in the Sinjar Trough, where it is 350 m thick in Well Kor Mor-3, 250 m in Well Chamchamal-1, 237 m in Well Kirkuk-107, 170 m in the Khabbaz Field, 125 m in Well Butmah-1, and finally 198 m in Well Tel-Hajar-1 (Al-Qayim et al., 2010; Sahar, 1987). The Mauddud Formation passes laterally into the Balambo Formation in north-eastern Iraq and to the Upper Sarmord or Jawan formations on the Mosul High (Jassim and Buday, 2006).

Figure 2. Stratigraphic correlation section of the studied formations in north-western Iraq and north-eastern Syria (modified after Al-Naquib, 1967; Kaddouri, 1982).

The Mauddud Formation in Well Az-16 of the Ain Zalah oilfield consists of a single stratigraphic unit (lithofacies 1) of 92 m of dark gray dolostone with fracturing and oil shown throughout the section; the upper contact of the formation is disconformable with abrupt changes in facies to recrystallised and fossiliferous limestone of the Gir Bir Formation, whereas the lower contact is conformable with marly dolostone of the Sarmord Formation (Figure 3).

The Wajnah Formation (Upper Santonian-Lower Campanian) was described first by Chatton in 1962 from Well Ain Zalah-19 as 15 m of lagoonal carbonate facies consisting of dolomite and fine grained limestone with abundant ostracods, a *Glomospira* fauna, and orbitoid foraminifera such as *Monolepidorbis* (*Praeorbitoides*), and is associated with anhydrite nodules in some places. These pass to marly limestone with depth and become

conglomeratic marly limestone at the contact with the underlying Gir Bir Formation (Chatton, 1997; Aqrawi et al., 2010).

The Wajnah Formation at the Ain Zalah oilfield consists of three lithofacies. (i) Lithofacies 1 consists of conglomeratic limestone which is composed of rounded to subrounded granules (>2 mm) within brownish to gray limestone. This lithofacies represents the lower stratigraphic unit at the Ain Zalah field that overlies the Gir Bir Formation. (ii) Lithofacies 2 consists of grayish brown, hard microcrystalline limestone occasionally associated with stylolite and fractures. This lithofacies represents the stratigraphic units 2 and 4 as (67.8%) of the total Wajnah Formation thickness at well Az-16. (iii) Lithofacies 3 is characterised by dark gray dolomite and dolomitic limestone of 12 m thickness as stratigraphic Unit 3 in Az-16 with oil shows and fracturing effect in the upper part of the unit (Figure 3).

The oligosteginal limestone of the Mushorah Formation overlies the Wajnah Formation with conformable contact, where the facies gradually changes from lagoonal facies below to the oligosteginal limestone above. By contrast, the Wajnah Formation's lower contact is erosional, disconformable, and taken at the contact between the basal conglomerate and the underlying brecciated and recrystallised limestone of the Gir Bir Formation (Aqrawi et al., 2010).

Figure 3. Stratigraphic units of the Butmah Formation in well Bm-15 (left), the Mauddud (top right) and Wajnah (bottom right) formations in well Az-16. Where U= Stratigraphic unit, L= Lithofacies.

4. Observed dolomitisation models

Each of the studied formations is characterised by different types of dolomite crystal, textures and degrees of cementation effect which conspire to reflect the provenance of their dolomitisation. Three dolomitisation models have been identified as operating in these formations: (i) reflux dolomitisation, (ii) mixing zone dolomitisation, and (iii) burial dolomitisation.

The three studied formations were deposited in tidal flat and lagoon environments (inner platform) that are considered chemically conducive to dolomitisation, where their salinity is above thermodynamic and kinetic saturation with respect to dolomite. Dolomitisation in these environments depends on a sufficient supply of magnesium, and thus on hydrologic parameters. Most massive dolostones have been interpreted to be formed according to the freshwater/seawater mixing model and/or the sabkha with reflux model (Machel and Mountjoy, 1986).

The reflux dolomitisation model was first suggested by Hsu and Siegenthaler (1969) to interpret dolomitisation in a dry climate supratidal environment, where dolomitisation is caused by lateral reflux of marine water. Where evaporation is high, this environment retains Ca^{2+} and incorporates it with SO_4^{2-} to create gypsum $CaSO_4(H_2O)_2$, which is subsequently converted to anhydrite $CaSO_4$ after dehydration which occurs upon burial. These processes increase the Mg^{2+}/Ca^{2+} ratio in the interstitial water, leading to dolomitisation and creating aphanotopic and fine to medium mosaic dolomite textures. These textures, with contemporaneous anhydrite cement, are commonly observed in the Butmah Formation as (i) anhydrite nodules associated with aphanotopic or fine crystalline dolomite, (ii) fenestral pores occluded by anhydrite cement within dolomite lithofacies (Figure 4A), (iii) sparse anhydrite crystals within fine crystalline dolomite (Figure 4B this), and (iv) chicken-wire dolomite textures (Figure 4C), and have $\delta^{13}C$ values ranging from 2.25‰ to 3.06‰ (PDB) and $\delta^{18}O$ from -3.21‰ to -2.44‰ (PDB) (Table 1). These features represent powerful evidence for this model (Warren, 2000; Machel, 2004; Mleali et al., 2013; Zhang et al., 2017; Ren et al., 2017).

Table 1. Carbon and oxygen isotope data from the Butmah, Mauddud and Wajnah formations.

Formation	Units	Lithofacies	Sample	$\delta^{13}C$ ‰ (PDB)	$\delta^{18}O$ ‰ (PDB)	Z (Salinity index)	Genesis/ Model
Butmah	U.4	L.3	B1	2.25	-2.44	130.70	Seepage reflux
			B2	3.06	-3.21	132.11	
Mauddud	U.1	L.1	M1	3.72	-6.73	131.09	Moderate to deep burial
			M2	2.58	-7.38	128.87	
Wajnah	U.3	L.3	W1	1.38	-2.63	128.97	Shallow burial
			W2	1.59	-3.06	129.24	

$Z = 2.048 \times (\delta^{13}C + 50) + 0.498 \times (\delta^{18}O + 50)$ (PDB), Values of $Z < 120$, is freshwater carbonate rocks, and when $Z = 120$, an unfinalized carbonate, Whereas, $Z > 120$ indicate marine carbonates (Keith and Weber, 1964).

The mixing zone model is used to explain subtidal platform dolomite that is not associated with evaporate minerals. It was used first by Hanshaw et al. (1971) to explain the presence of dolomite in Tertiary carbonate aquifers in Florida (Warren, 2000). The principle of the model depends on mixing fresh or meteoric water with marine water within lagoon environments (Morrow et al., 1986). Fall in sea level creates good conditions for the mixing mechanism of meteoric water with marine water within the mixing zone. This model has been noted commonly in the Mauddud and Wajnah formations. The very fine to fine crystalline textures of the Wajnah Formation are not associated with anhydrite reflux to early dolomite nucleation within a hyposaline subtidal environment (Machel, 2004). By contrast, the planar-e to planar-s dolomite crystals ranging in size from 1 to 100 µm that commonly show cloudy centres surrounded by clear, limpid rims in the Mauddud Formation represent one of the descriptive features of the mixing zone model (Kyser et al., 2002) (Figure 4D). Furthermore, the dolomite crystals that occur as cement fill voids, mould and vugs in mosaic dolomite textures in the Wajnah and Mauddud formations may be related to this model (Kaldi and Gidman, 1982; Ward and Halley, 1985). The $\delta^{13}C$ values were found to range from 1.38‰ to 1.59‰ (PDB) and $\delta^{18}O$ from 3.06‰ to -2.63‰ (PDB), indicating a shallow burial origin (Table 1).

The burial dolomitisation model was first suggested by Illing (1965) as subsurface dolomitisation under deep burial due to the alteration of clay minerals (Warren, 2000), and is also called the burial-compaction model (Morrow, 1982). In this model increasing burial depth extracts the interstitial water from the deposits, with subsequent dolomitisation taking place under preferential conditions of temperature, pressure and Mg^{2+} concentration (Machel, 2004).

Late dolomitisation was characterised in this study by (i) Coarse planar-s dolomite crystals as a result of slow replacement of precursor limestone in the presence of early burial compaction fluid during shallow to intermediate burial; (ii) Coarse planar-s to nonplanar-a dolomite crystals formed at high temperature and deep depth reaching to more than 2 km. Saddle or baroque dolomite textures associated with stylolites are among the most important features of the deep burial dolomitisation model (Amthor and Friedman, 1992; Machel, 2004). In this paper, both coarse crystalline dolomite and saddle dolomite were recorded in the Butmah, Mauddud and Wajnah formations (Figure 4E and Figure 4F). Partial dolomitisation occurring on stylolite surfaces may change to comprehensive dolomitisation when the solution becomes saturated in Mg^{2+}, explaining the comprehensive subsurface dolomitisation that sometimes occurs in the carbonate platform (Warren, 2000). The $\delta^{13}C$ values were found to range from 2.58‰ to 3.72‰ (PDB) and $\delta^{18}O$ from -7.38‰ to -6.73‰ (PDB), which indicated that they have a moderate to deep burial origin (Table 1).

In terms of early and late dolomitisation, the reflux dolomitisation model that was characterised in the Butmah Formation and the very fine and fine dolomite crystals of the Wajnah Foramtion are examples of early dolomitisation, whereas the other features of the mixing zone model and the burial dolomitisation model were described as late dolomitisation.

Figure 4. Experimental petrogtaphic evidence of diagenetic processes. A: Fenestral pores (f) occluded by anhydrite cement as early cementation in the Butmah Fm., Bm-15, (2488 m). B: Sparse anhydrite crystals (s) within fine crystalline dolomite in the Butmah Fm., Bm-15 (2422 m). C: Compressed chicken-wire texture (c) caused by compaction, Butmah Fm, Bm-15, (2379 m). D: Cloudy dolomite centres (c) surrounded by a clear limpid rim, Mauddud Fm., Az-16, (2446 m). E: Zoned coarse dolomite crystals (z) as late dolomitisation features in the

Mauddud Fm., Az-16, (2472 m). F: Saddle dolomite (s) as a late dolomitisation feature associated with stylolite and oil shows (o), Mauddud Fm., Az-16, (2486 m).

5. Experimental Results

A reservoir unit is a rock with enough porosity for storage of hydrocarbon (oil and gas) inside its pores and permeability to permit its movement (Sadeq and Wan Yusoff, 2015). Hence, the pore space of the rock must be interconnected to move the hydrocarbon through the reservoir unit, and the reservoir hydrocarbon should be present in commercial quantities (Sadeq and Wan Yusoff, 2015). Consequently, the petrophysical properties of the studied formations considered by this study include porosity, pore throat, pore and crystal size distributions, qualitative pore network description, and permeability.

5.1 Porosity

Porosity is a measure of storage capacity of a reservoir. It is defined as the ratio of the pore volume to bulk volume (Tiab and Donaldson, 2012). The porosity of carbonate reservoirs can vary from little more than 0% in tightly cemented carbonate rock to about 40% for unconsolidated sediments (Gluyas and Swarbrick, 2004).

The effective porosities that were measured using helium porosimetry in this study are presented in Table 1 and Figure 5. The highest porosity in the Butmah Formation was 8.27%, and the lowest 0.72%, with an arithmetic mean of 4.20%, and a mode of 3.5%. Figure 5 shows that the porosity distribution of the Butmah Formation is approximately unimodal (allowing for the effects of unbalanced binning) with a wide spread (standard deviation = 4.52%).

Table 1. Statistical analysis of the effective porosity of the dolomitised units of the Butmah, Mauddud and Wajnah formations.

Formation	Units	Lithofacies	Number of samples	Effective porosity (%)				
				Min	Max	Mean	Mode	Std Dev
Butmah	U.4	L.3	24	0.72	8.27	4.20	3.5	4.52
Mauddud	U.1	L.1	20	2.44	9.21	5.63	5.0	3.92
Wajnah	U.3	L.3	20	2.80	9.69	5.94	5.5	3.62

The porosity distribution of the Mauddud Formation is unimodal (Figure 5) with a modal value in the range 4.0% – 6.0% (40% of the 20 samples measured) and ranging from 2.44% to 9.21%, as shown in Table 1. Unit 3 in the Wajnah Formation (Figure 5) also shows a unimodal porosity distribution ranging from 2.80% to 9.69%, with a modal value in the range 5.0% – 6.0%, representing 25% of the 20 samples available. The porosity mean and mode of the Wajnah Formation are 5.94% and 5.5% respectively, as shown in Table 1.

Consequently, the effective matrix porosity of all of the studied formations is less than 10%, but varying widely, from 0.72% – 8.27% for the Butmah Formation and 2.44% –.9.21% for the Mauddud Formation, whereas the Wajnah Formation showed a porosity distribution from 2.8% to 9.69%.

Figure 5. Histograms of the effective porosity of the Butmah Formation at Well Bm-15, the Mauddud Formation, and the Wajnah Formation at Well Az-19.

5.2 Pore throat, pore size and crystal size distributions

A combination of the natural wettability of the matrix mineral–fluid interface and the size of constrictions within the pore network results in wetting fluids remaining in small pores (Tiab and Donaldson, 2012). The capillary force, which keeps the wetting fluid within the small pores, must be counteracted if one is to remove the fluids from such pores, and depends on the interfacial tension, wetting angle and pore throat size. The first two of these parameters depend upon temperature and to a small extent on fluid pressure, whereas the latter is sensitive mainly to effective pressure which can act to reduce pore throat sizes and reduce pore interconnection (Bjørlykke, 2010; McPhee et al., 2015). Consequently, wettability and capillary pressure partially control the relative permeability of a reservoir rock (Ahr, 2008; Bjørlykke, 2010; Tiab and Donaldson, 2012).

In this work, MICP analysis has shown differences in the pore throat and pore size distribution within the three studied formations. These differences in the pore network are governed by the dolomite recrystallisation, anhydrite occurrences and subsequent diagenesis. Ten

samples were selected from the studied formations for MICP analysis (4 samples for the Butmah Formation, and 3 samples each for the Mauddud and the Wajnah formations). The pore throat distributions from some of these samples are shown in Figure 6.

Samples from the Butmah Formation (Unit 4) showed a wide range of pore sizes, with pores as small as 2 nm and as large as 10 µm. These samples exhibit poor pore sorting, and may be unimodal or multimodal. The two examples given in Figure 6 show very different behaviours; one having two very clear peaks at about 20 nm and 20 µm, while the other has a single broader peak at approximately 0.5 µm. Clearly, dolomitisation has left different parts of this formation with significantly different pore textures when assessed by pore throat diameter.

By contrast, samples from the Mauddud formation (Unit 1) exhibit a single, broad peak. The two examples in Figure 6 show slightly different styles, one exhibiting a single peak at about 0.5 µm, with very few pores greater than 5 µm or less than 20 nm, the other having a peak at 20 nm, but significant pore throat sizes up to about 1 µm. Once again, the variability in the data depends on the local operation of different dolomitisation processes.

Finally, samples from the Wajnah Formation (Unit 3) show very well defined unimodal distributions, again with the variability in the modal values of the pore throat diameters. Data from the two examples given in Figure 6 show one with a peak at a diameter of about 0.4 µm and one at about 0.07 µm.

Figure 6. Pore throat distributions for six samples subjected to MICP measurements. Top row (A) and (B): two samples from the Butmah Formation. Middle row (C) and (D): two from the Mauddud Formation. Bottom row (E) and (F): two samples from the Wajnah Formation.

MICP results were used to characterise pore size distributions using the Glover and Dery (2010) method, whereas the Glover and Walker (2009) method was used to derive the crystal size distributions that show good agreements with the results of using the optical petrographic

microscope (OPM) and scanning electron microscope (SEM) imaging for describing the pore and crystal size.

The Luo and Machel (1995) classification was used for classifying the pore size. This classification can be used for both limestones and dolostones and has a wide range from very large pores that can be characterised by the naked eye (more than 256 mm), such as karst caverns, to the very small pores that are measured by scanning electron microscopy (SEM) and mercury injection capillary pressure (MICP) (less than 1 μm).

Figure 7 shows the resulting classified pore size distribution within the three studied formations. The Butmah and Mauddud Formation histograms show unimodal pore size distribution ranging from <0.2 to 4000 μm with a modal pore size in the range 0.2-1 μm (33% and 34% respectively). Whereas the Wajnah Formation histogram shows a pore size distribution range between <0.2 and 1000 μm, exhibiting a modal value in the pore size range of 0.2-1 μm (44%).

Figure 7. Histograms of pore size distribution within the Butmah, Mauddud, and Wajnah formations using pore size bins defined by the Luo and Machel (1995) classification.

The use of crystal size scales allows more extensive differentiation of dolomite fabrics. Different crystal size limits were developed by Folk (1962), Friedman (1965), Randazzo and Zachos (1984) and Wright (1992).

In this study, we used the Folk (1962) terms 'very fine crystalline dolomite' for crystal size less than 4-16 μm, 'fine crystalline dolomite' for crystal size from 16–62 μm, 'medium crystalline dolomite' for crystal size from 62-250 μm, 'coarse crystalline dolomite' for crystal size from 250-1000 μm, and 'very coarse crystalline dolomite' for crystal size more than > 1000 μm.

Figure 8 shows crystal size distribution within the three studied formations. Wide crystal size distributions were recorded as a unimodal histogram in the Butmah Formation, ranging from less than 16 μm to more than 1000 μm with mode (32%) in the range 62-250 μm. The Mauddud Formation shows a unimodal histogram within crystal size distribution range 16-62

μm and more than 1000 μm with mode at the crystal size range 250-1000 μm (42%). Whereas the Wajnah Formation histogram shows a unimodal shape but with lower crystal size ranges represented by crystal size less than 16 μm to 250 μm and mode (54%) at the crystal size range 16-62 μm.

Figure 8. Histograms of crystal size distribution within the Butmah, Mauddud, and Wajnah formations using crystal size bins defined in this work.

5.3 Pore network description

The porosity of the studied formations was described and classified based on the Choquette and Pray (1970) classification and Lucia's (1983, 1995) classification for pore type description. The Luo and Machel classification was used for identifying the pore size distribution and the Ahr (2008) classification was used for characterising the final shape of the pore network and pore system of the studied formations.

Combining previous measurement data with qualitative micrography using both polarising microscopes and SEM has allowed us to characterise the pore network of each of the studied formations.

The Butmah Formation (Units 2 and 4) consists of vugs (Vg), intercrystalline (Inc), and microfractures (Mf) (Figure 9). These pores depend on dolomite crystallisation and occurrence of anhydrite cement between the dolomite crystals. This lithofacies has a good porosity when the anhydrite cement is diagenetically dissolved, exhibiting a variety of pore sizes from large mesopores (62.5 μm – 1mm) to small micropores (<2 μm). The smaller pores are in the form of intercrystalline spaces, which are generally well-connected, whereas the larger ones are often in the form of isolated vugs that may occasionally be connected. Some of these vugs are large, of the order of 0.5 mm, which can be seen as open macropores in Figure 9D, shown by the blue dyed epoxy with which they are injected, and as anhydrite filled macropores in Figure 10A, where they can be recognised as the large, white, uniformly-filled patches on the micrograph.

The intensity of fracturing in all the stratigraphic units of the Butmah Formation is high, but most of the fractures have been completely or partially occluded, commonly by anhydrite cement and occasionally by calcite cement. Nonetheless, some open fractures do exist in the formation, especially in Unit 4 (Figure 10A).

Unit 3 of the Wajnah Formation contains pores ranging from large mesopores (62.5 μm – 1 mm) to small micropores (<2 μm), in the form of intercrystalline pores and vugs and some biomoulds, as shown in Figure 10B, 10C & 10E. The fracture intensity is high in Unit 3, and some of the open fractures show traces of oil. Consequently, the predominant pore network in Unit 3 of the Wajnah Formation results from a combination of dissolution, dolomitisation and fracturing processes.

The Mauddud Formation consists entirely of dolomite units. The existing dolowackestone has large mesopores (62.5 μm – 1 mm) which exhibit as vugs and intercrystalline pores, whereas the coarse crystalline dolomite texture has fewer intercrystalline pores whose size extends as far as small micropores (<2 μm). The floating-contact rhomb dolomudstone has some vugs, as shown in Figure 10D & 10F. Fracturing is moderate in the Mauddud Formation, and some of these fractures are either partially or completely closed by calcite cements.

The resulting pore network in the Mauddud Formation indicates that in Unit 1 pores within the three characterised microfacies are created due to a combination of dissolution, dolomitisation and fracturing.

Table 2: The pore system of the studied formations according to their pore type, pore size and crystal size.

Formation	Units	Lithofacies	Crystal size (μm)	Pore type	Pore size (μm)	Pore system
Butmah	U.4	L.3	<16 - >1000	Vg, InX, Mf	<0.2 – 4000	D & H (d-f)
Mauddud	U.1	L.1	16 - >1000	Vg, InX, Mf	<0.2 – 1000	H (d-f)
Wajnah	U.3	L.3	<16 - 250	Vg, InX, Mf	<0.2 – 1000	H (d-f)

Notes: Vg=vugs, InX=intercrystalline, Mf= microfractures, D=diagenetic system, H (d-f)=hybrid (diagenetic-fracturing) system.

Figure 9. A: Intercrystalline porosity (i) and vuggy porosity (v), Butmah Fm., Bm-15, U.4 (2450 m). B: Vuggy (v) and fractures (f) porosity, Butmah Fm., Bm-15, U.4 (2450 m). C: intercrystalline porosity (i), Butmah Fm., Bm-15, U.2 (2597 m). D: vuggy (v) and intercrystalline (i) porosity of medium dolomite crystals, Mauddud Fm. Az-16, U.1, (2452 m). E and F: are SEM images showing pore shape and size in 2D and 3D, respectively, for a sample from the Butmah Fm., Bm-15, U.4 (2388 m).

Figure 10. A: Fracture porosity (f) and anhydrite cement occluding intercrystalline (oi) and vuggy pores (ov), Butmah Fm., Bm-15, U.4 (2450 m). B: very fine crystalline dolomite with some vugs (v) and intercrystalline (i) pores, Wajnah Fm., Az-16, U.3 (2349 m). C: Intercrystalline porosity (i) of fine crystalline dolomite, Wajnah Fm., Az-16, U.3 (2351 m). D: intercrystalline (i) and vuggy (v) porosity of medium dolomite crystals, Mauddud Fm., Az-16, U.1, (2484 m). E: intercrystalline porosity, Butmah Fm., Bm-15, U.2 (2597 m). F: SEM images showing pore shape and size in 2D in the Wajnah Fm., Az-16, U.3 (2350 m) and Mauddud Fm. Az-16, U.1 (2453 m), respectively.

5.4 Permeability

There are three main diagenetic factors which control the permeability of carbonate rock, namely, cementation, dissolution and fracturing (Tiab and Donaldson, 2012). One of the goals of the research presented in this paper is to examine to what extent each of these diagenetic factors controls permeability in the studied formations.

During the measurement and analysis of laboratory obtained permeability data, it is extremely important to be aware of systematic errors. Specifically, it is important to recognise that permeability data obtained by core analysis always represent the lower limit of permeability, especially in fractured units. Core plugs chosen for core analysis are always taken from well-indurated rocks rather than fractured sections in order to obtain a whole sample for the measurement. Unfortunately, this automatically leads to permeability measurements from core data being unrepresentative, generally underestimating permeabilities one would find in the real fractured rock.

In this study, permeability measurements were carried out using helium gas permeametery measurements using a pulse-decay method. Summary results are presented in Table 3 and Figure 11.

Table 3. Permeability measurements of the studied formations.

Formation	Units	Lithofacies	Number of samples measured	Matrix permeability (mD)		
				Min	Max	Arithmetic Mean
Butmah	U.4	L.3	24	5.41×10^{-5}	4.53×10^{-2}	5.14×10^{-3}
Mauddud	U.1	L.1	20	8.50×10^{-4}	8.64×10^{-2}	2.00×10^{-2}
Wajnah	U.3	L.3	20	6.31×10^{-4}	1.75×10^{-2}	3.36×10^{-3}

The permeabilities of all formations fall in the range one might describe as a tight carbonate. The lowest permeability in the Butmah Formation is 5.41×10^{-5} mD and the highest is 4.53×10^{-2} mD, with a mean of 5.14×10^{-3} mD. Figure 11 shows that the permeability in the Butmah Formation is distributed between 1.0×10^{-1} mD and 1.0×10^{-5} mD, with the highest occurrence (37.5% of the measurements) in the range 1.0×10^{-3} mD – 1.0×10^{-4} mD.

By contrast, the permeabilities for the Mauddud Formation cover a more restricted range (1.0×10^{-1} mD to 1.0×10^{-4}) towards the top of the range occupied by the Butmah Formation, with highest occurrence of permeability (50% measurements) being recorded in the range 1.0×10^{-2} mD – 1.0×10^{-3} mD. The mean permeability in the Mauddud Formation is 2.0×10^{-2} mD and the highest and lowest values were 8.64×10^{-2} mD and 8.50×10^{-4} mD, respectively. The permeability of the Wajnah Formation is similar to that of the Mauddud Formation, but a little tighter. The mean permeability in the Wajnah Formation was found to be 3.36×10^{-3} mD, with the highest permeability 1.75×10^{-2} mD and the lowest 6.31×10^{-4} mD.

Figure 13. Permeability histograms of the Butmah Formation at Well Bm-15, the Mauddud Formation and Wajnah Formation at Well Az-19.

6. Discussion

6.1 Dolomitisation and poroperm relationships

The permeability of tight carbonate rocks depends on porosity in a similar way to other porous rocks (Rashid et al., 2015a). Plotting the permeability against porosity, however, does not produce a straight line. Furthermore, any given formation gives rise to a cloud of points that

follow a trend rather than a single curve. In general, that curve follows a power law with respect to porosity. There are many models which define the exponent to that power law, of which one of the most recent is the RGPZ model, where a permeability prediction equation has been developed for clastic sandstone reservoir rocks using the electrical conductivity of a porous media, and based on the effect of porosity, grain size and cementation fraction on and pore connectivity fluid flow (Glover et al., 2006).

In the RGPZ model the permeability is directly proportional to the porosity raised to the power of an exponent equal to 3 times the cementation exponent in Archie's first law (Glover, 2010; 2015). The existence of a cloud of points rather than a single curve is explained by other parameters in the RGPZ equation, which together with the cementation exponent describe how the permeability of any formation for a given porosity also depends upon how well the pore spaces connected. The most important of these other parameters are grain diameter in clastic rocks (Glover et al., 2006) and pore diameter in carbonates (Rashid et al., 2015b).

The relevance of the RGPZ equation to tight carbonates has been studied previously (Rashid et al., 2015a; 2015b). These authors recognised that an assumption at the heart of the theoretical RGPZ equation was valid only for clastic rocks, and subsequently modified the original theoretically derived RGPZ equation to produce a version valid for high permeability and tight carbonates.

Table 4 shows summary poroperm data for each formation, whereas Figure 12 shows the data measured in this work plotted on a poroperm diagram. Conventionally, the porosity is plotted on the x-axis on a linear scale, whereas the permeability is plotted on the y-axis using a logarithmic scale. As expected, permeability increases by orders of magnitude as porosity increases, at a rate of approximately one order of magnitude per 2% porosity increment.

Table 4: Summary of the poroperm data of the studied formations.

Formation	Porosity (%)	Permeability (mD)	Pore throat (μm)
Butmah	0.72 – 8.27	5.41×10^{-5} – 4.53×10^{-2}	0.007 – 12
Mauddud	2.44 – 9.21	8.50×10^{-4} – 8.64×10^{-2}	0.009 – 14
Wajnah	2.80 – 9.69	6.31×10^{-4} –1.75×10^{-2}	0.02 – 2

Figure 12. Porosity - permeability relationships of the Butmah, Mauddud and Wajnah formations, showing the distribution of pore throat diameter, crystal size, and amount of cement. In the blue cement amount bar L = low, M= moderate, H= high. In the orange crystal size bar F= fine crystals, M= medium crystals, C= coarse crystals, and VC= very coarse crystals.

Figure 12 also shows pore throat diameter and categorisation for crystal size, degree of cement and lithofacies. Increase in cementation is associated with a reduction in pore throat diameter as expected. However, further deterministic associations should not be read into the categorisations. For example, fine crystal size is not necessarily related to a high degree of cementation, but both are associated with smaller pore throat diameters.

Figure 12 further shows overlaid curves for the original RGPZ model for four different combinations of parameters. Each of these combinations keeps the cementation exponent constant (m=2), and varies the crystal size from 10 µm to 300 µm. Increasing the cementation exponent translates the curves towards lower permeabilities, i.e., downwards, while increasing the crystal size increases permeabilities as shown. The tight carbonate version of the RGPZ model includes a third parameter. Consequently, it is not possible to fit either the original or the tight carbonate models to the data without a further constraint, such as knowing the cementation exponent and modal crystal size. However, the overlay curves show that the data approximately conform to reasonable values for the model parameters.

Both the Mauddud and Wajnah formations show a relationship between permeability and porosity with the degree of scatter one would expect from a single formation. The scatter in these data is defined by differences in crystal size and the connectivity of pores from sample to sample. By comparison, the Butmah Formation shows a very wide distribution of data

points which is very unusual for a single formation, and is an indicator that this formation is more heterogeneous than the others.

Very high permeability at low porosities is usually associated with fractured samples, whereas low permeabilities at relatively high porosities indicate a pore microstructure which has limited connectivity and is most often associated with cementation. It would be very difficult to fit the data from the Butmah Formation to an RGPZ model without invoking a wide range of crystal sizes and/or cementation exponents.

6.2 Dolomitisation and timing

Two main mechanisms of dolomitisation were characterised in this paper that are focused on the initial dolomitisation model, whether it is alone or associated with cementation (most likely anhydrite cement), to then show the subsequent diagenesis effects that are represented by recrystallisation, dissolution, cementation, and fracturing.

We have compared the quantitative and qualitative data arising from each of the formations with the requirements of the three dolomitisation types described earlier. Reflux dolomitisation is considered to be applicable to the Butmah Formation, whereas the mixing zone dolomitisation model is applicable to the Mauddud and Wajnah formations, and burial dolomitisation has been found to be consistent with all three formations.

Early dolomitisation represented by the reflux dolomitisation model combined with late dolomitisation and associated anhydrite precipitation leads to heterogeneous reservoir properties and a variable reservoir quality that is complex to predict. Lucia (1999) noted that anhydrite nodules and poikilotopic anhydrite textures produced only minor effects on the poroperm relationship in the South Cowden carbonate rocks of West Texas. Moreover, anhydrite fabrics have sometimes been found to improve reservoir quality (Lucia, 2004). According to Figure 12, the lowest permeability and porosity samples, found only in the Butmah Formation, represent the effects of early dolomitisation resulting from reflux dolomitisation (dolomitisation with anhydrite cement), and give the worst reservoir properties.

Whereas, the very fine and fine dolomite crystal samples of the Wajnah Formation show better porosity and permeability as a result of the early dolomitisation mixing zone model.

The Wajnah Formation samples also exhibit late dolomitisation or a combination of early and late dolomitisation represented by mixing zone dolomitisation and burial dolomitisation, although the Mauddud Formation has been subjected to late dolomitisation alone (mixing zone and burial dolomitisation).

The best reservoir properties are due to the effect of both early and late dolomitisation and represented by some samples from the Butmah Formation which have undergone early reflux dolomitisation followed by later shallow burial dolomitisation, and consequently have both higher porosities and permeabilities as the result of greater connectivity of larger pore throats due to late dissolution of the associated anhydrite cement. These reservoir qualities were also found in the Mauddud and Wajnah formations where early or late mixing zone dolomitisation followed by later shallow burial dolomitisation with no cementation are the causes.

By contrast, the worst reservoir quality in the Mauddud Formation samples is due to late dolomitisation and represented by the deep burial dolomitisation that shows saddle dolomite textures associated with stylolites.

6.3 A new dolomite pore network architecture model (PNAM)

Clearly, the interplay between different diagenetic processes occurring at different times controls the pore network architecture in a complex way. For example, in the Wajnah Formation, the dolomite crystals simply increase from fine crystalline dolomite to medium crystalline dolomite, which improves the reservoir quality. However, increase in the dolomite crystals' size in the Butmah Formation from fine crystalline dolomite to coarse crystalline dolomite affects the reservoir quality in two opposing ways: (i) positively, by increasing permeability in those parts of the rock matrix which have no associated anhydrite cement, and (ii) negatively, where the anhydrite cement occludes the intercrystalline pores in the samples, as shown in Figure 13. Such co-dependencies of reservoir quality upon multiple

diagenetic processes are common in dolomitised carbonate reservoirs. We have developed a pore network architecture model (PNAM) to help understand these co-dependencies.

Figure 13. Recrystallisation versus dissolution and cementation effects on the reservoir properties and heterogeneity of the studied formation samples.

Figure 13 shows the new pore network architecture model for dolomite reservoirs according to the main effective diagenetic processes. In this figure, crystal size increases upwards and cementation increases towards the right. Consequently, the process of cementation alone moves a rock texture horizontally right in the diagram, whereas cementation with recrystallisation results in a move to the right and upwards. Recrystallisation alone, whether due to early or late dolomitisation, moves the rock texture upwards vertically to a texture with a larger crystal size, whereas recrystallisation with dissolution moves the rock texture upwards and to the left in the diagram. The operation of dissolution on its own moves the rock texture horizontally to the left in the diagram.

High reservoir quality is represented by the textures on the left-hand side of the figure, particularly towards the top, whereas low reservoir quality rock occurs on the right of the diagram, particularly towards the bottom. Hence reservoir quality increases diagonally towards the top left.

Cementation generally reduces the reservoir properties (pore throat, porosity, and permeability) and can do so even if recrystallisation is increasing the crystal size because it will fill the larger pores sizes between the enlarged crystals. Similarly, dissolution increases reservoir quality by increasing pore throat diameters, porosity and permeability, and will do so more effectively if occurring in tandem with recrystallisation. Heterogeneous rock textures occur in the centre of the figure, implying that homogeneity is not necessarily associated with good reservoir quality in carbonate rocks. We will discuss this observation in more detail in the following subsection.

Applying the new model to the Mauddud Formation shows that the reservoir quality is improved by increasing the dolomite crystal size from fine crystalline dolomite to coarse crystalline dolomite, then degraded again by further increases in the size of the dolomite crystals from coarse crystalline dolomite to very coarse crystalline dolomite because the previous improvements in reservoir quality allowed the ingress of mineral-rich fluids which have led to partial cementation of the newly available larger pore space.

The cementation effect is clear in the Butmah Formation, affecting the reservoir quality of the measured dolomite samples strongly, whereas it is less pronounced in the Wajnah Formation and low in the Mauddud Formation.

6.4 Diagenesis, heterogeneity and cementation in the PNAM

In general, a carbonate reservoir formation will have complex spatially-distributed petrophysical parameters including porosity and permeability (Glover et al., 2018), which vary over a wide range of scales (Lucia,1995; Lønøy, 2006; Ehrenberg et al., 2008; Hollis et al., 2010). This already complex picture is complicated further by the interaction between different diagenetic processes and the timing in which they occur.

In this study, both early and late dolomitisation have been identified within each of the three dolomitisation models. Early dolomitisation was found to occur in sabkha and hypersaline environments with widespread pore-filling by anhydrite cement in Unit 4 of the Butmah Formation. The dolomitised samples containing anhydrite show a wide range of heterogeneity in the pore network dependent upon the degree of anhydritisation. In these rocks, early dolomitisation produces a rock which occurs in the centre-left of the PNAM and exhibiting low heterogeneity. Subsequent anhydritisation moves the rock towards the right in the PNAM, resulting in higher heterogeneity and lower reservoir quality.

By contrast, rocks exhibiting early dolomitisation without associated anhydrite (such as in the Wajnah Formation) show low heterogeneity in the pore network on the left-hand side of the PNAM, with reservoir quality dependent upon the crystal size. Rocks composed of fine crystals (bottom left in the PNAM) are homogeneous and of relatively low reservoir quality

because they are tight. However, the reservoir quality increases upon later dolomitisation, resulting in recrystallisation that provides larger crystal sizes. The process results in the rock moving vertically in the PNAM, from the bottom left upwards. This process retains the homogeneity of the rock providing that the dolomitisation is widespread. However, if dolomitisation is patchy, the heterogeneity of the rock will increase and the resulting rock will not have as high a reservoir quality as it otherwise would have had.

The Mauddud Formation also shows low heterogeneity in the pore network, with an increase in reservoir quality as crystal size increases concomitant upon late dolomitisation, depicted by the same upward trend in the PNAM.

6.5 Diagenesis and reservoir types

Diagenesis can be caused by many processes including dolomitisation. Dolomitisation has been classified into two types according to their timing. Early dolomitisation may have resulted from a number of different scenarios, leading to the different dolomitisation types shown in Figure 3. Each of these dolomitisation types not only has a different provenance, but results in a different distribution of dolomitisation and differences in the petrophysical rock properties. Dolomitisation may have occurred alone or be associated with cementation. Indeed, later on, the rock may be subject to different diagenetic processes such as further dolomitisation, recrystallisation, dissolution, cementation, compaction and fracturing. In other words, many different diagenetic processes occurring at different times may conspire to produce the final pore network. The picture is further complicated by the interplay between different diagenetic processes which can amplify or limit each other.

We have combined all of the previous information reported above to define six reservoir types (R_i) for dolomitised formations which are process-driven, as shown in Figure 14. Each of these Process Driven Reservoir Types (PDRTs) may have also undergone dolomite cementation at the end of the late dolomitisation phase to give an additional six reservoir types (R_{ci}), where *i* is the reservoir type number. Despite this being yet another dolomitisation

classification, we hope that the process-driven nature of the classification will be the first step to a full quantification of the effects of dolomitisation and any associated cementation. The result of each of the processes in Figure 14 can be found by referring to the pathway the texture of the rock and the pore network follow in the PNAM (Figure 13).

Figure 14. Flow chart showing the process-driven outcome reservoir types (PDRTs) for dolomitised rock.

As mentioned earlier, all dolomite rocks can be separated into those where early dolomitisation occurs alone (PDRTs R1 to R3 in Figure 14) and those where early dolomitisation is associated with cementation (PDRTs R4 to R6).

It is worth noting that the PDRTs are also an indicator of reservoir quality, with reservoir quality decreasing as the PDRT number increases and with the addition of the 'c' qualifier. Consequently, the best reservoir quality is R1 and the worst is Rc6. When the rock is affected by early dolomitisation alone, three types of reservoir rocks can be identified according to the effect of the subsequent diagenesis.

In the first, recrystallisation and dissolution improve the petrophysical properties, increasing porosity, widening pore throat sizes, improving pore connectivity, and significantly augmenting permeability (R1, Rc1, R4, and Rc4 in Figure 14).

In the second, recrystallisation occurs without dissolution, leading to improvements in the rock's petrophysical properties as in the first case but not to the same extent (R2, Rc2, R5, and Rc5 in Figure 14). The same result can be achieved by invoking recrystallisation together with coeval dissolution and cementation, each occurring to an extent sufficient to balance the effect of the other. A slight imbalance would clearly lead to a slight increase or decrease in reservoir quality depending, respectively, upon whether the dissolution or the cementation effect dominated.

The third type of dolomitised rock occurs through the linked processes of recrystallisation and cementation degrading the petrophysical properties of the rock. These processes decrease

porosity, narrow pore throat sizes and can lead to completely blocked pore throats. Subsequently, there are significant reductions in pore connectivity, and hence significantly reduced permeability (R3, Rc3, R6, and Rc6 in Figure 14). By contrast, recrystallisation and cementation reduce the reservoir properties of the origin rock (R3, Rc3) and (R6, Rc6).

Figure 16 shows that the main two mechanisms of dolomitisation are (i) dolomitisation and cementation and (ii) dolomitisation alone. The reservoir quality generally improves upward, where the last upper category of the dolomitisation and cementation mechanism suffers from dissolution but after dolomitisation generates with cement association as clarified in the Figure. When we turn from the lower category of the upper part in the dolomitisation alone mechanism, the first category suffers from cementation that may keep the reservoir quality the same as for the last category of the last mechanism. Then, turning to the upper part, the dolomite rock suffers from dissolution and cementation or neither of these and this generally creates better reservoir quality. Whereas, the best reservoir quality is found in the third category of the dolomitisation alone mechanism that shows the dolomitised rock suffering from dissolution after the dolomitisation.

The Butmah Formation is represented by PDRTs R4, R5, and R6, whereas the Wajnah Formation is represented by R2 and R3, and the Mauddud Formation exhibits varied PDRTs encompassing R2, Rc2, R3, and Rc3. Consequently, the reservoir quality of each unit in each field is not only clear but can be compared semi-quantitatively, analysed in well logs and even used as operational facies in geological modelling for reservoir simulation.

7. Conclusions

Cementation and dissolution are the main controls on the reservoir properties for many dolomite formations. These two major diagenetic processes work collectively with dolomite recrystallisation and fracturing to define the final pore network and control reservoir quality. We have carried out an extensive campaign of experimental measurements in order to characterise the link between ultimate rock microstructure and the diagenetic processes

which have caused it. The measurements were used to define 12 Process Driven Reservoir Types (PDRTs), each of which has been subjected to a different dolomitisation model, timing and their effect on the subsequent diagenetic processes and fracturing. We hope in future to validate the model further with greater amounts of data and continue to base the PDRTs on a quantitative footing.

Early dolomitisation plays a positive role in improving the reservoir properties, where it is not associated with anhydrite cement or dissolved later with burial, such as in the fine dolomite samples of the Wajnah Formation. The association of early dolomitisation with anhydrite cement leads to a more dispersed porosity-permeability relationship, as noted in the Butmah Formation, and reduces the permeability at any given porosity, as described in the Wajnah Formation. And hence, the early dolomitisation repesented by the reflux dolomitisation model creates variable reservoir properties (including porosity, permeability, and pore throat), normally either promoting reservoir compartmentalisation or leading to non-reservoir units and in a unique situation leading to conventional reservoirs, whereas the dolomite recrystallisation is the main factor controlling the reservoir properties in the mixing zone and burial dolomitisation models that have non-association with anhydrite cement.

A new dolomite pore network architecture model (PNAM) was developed in this study to illustrate the effects of cementation, dissolution, and recrystallisation with the dolomitisation on the reservoir pore network architecture. The model shows low pore network heterogeneity in the low and high cemented rocks, whereas the highest pore network heterogeneity was characterised in moderate cemented rocks. The model shows also that reservoir quality was affected by cementation more than recrystallisation.

Consequently, we define twelve reservoir types for dolomitised formations according to the dolomitisation types and the effects of different diagenetic processes such as further dolomitisation, recrystallisation, dissolution, cementation, compaction, fracturing, and dolomite cementation. Applying these Process Driven Reservoir Types (PDRTs) on the studied formations shows that the Butmah Formation is represented by R4, R5, and R6. The

Wajnah Formation exhibits R2 and R3, whereas the Muddud Formation is represented by R2, Rc2, R3, and Rc3.

Acknowledgements

The authors would like to thank the Iraqi ministry of oil represented by the North Oil Company for providing core samples and data, as well two anonymous reviewers whose comprehensive and incisive comments have improved the quality of the paper.

References

Adam, A.E., and Mackenzie W.S., 1998. A colour atlas of carbonate sediments and rocks under the microscope. Chemical rubber company (CRC) press, Oxford University Press, 184 p.

Agosta, F., Alessandroni, M., Antonellini, M., Tondi, E., Giorgioni, M., 2010. From fractures to flow: a field-based quantitative analysis of an outcropping carbonate reservoir. Tectonophysics ,490, p.197-213.

Ahr, W.M., 2008. Geology of carbonate reservoirs: the identification, description, and characterization of hydrocarbon reservoirs in carbonate rocks. Canada, John Wiley & Sons, Inc., Hoboken, New Jersey, 296 p.

Aleali, M., Rahimpour-Bonab, H., Moussavi-Harami, R., & Jahani, D. 2013. Environmental and sequence stratigraphic implications of anhydrite textures: A case from the Lower Triassic of the Central Persian Gulf. Journal of Asian Earth Sciences, 75, p.110-125.

Al-Qayim, B., Qadir, F. and Al-Biaty, F., 2010. Dolomitisation and porosity evaluation of the Cretaceous Upper Qamchuqa (Mauddud) Formation, Khabbaz oilfield, Kirkuk area, northern Iraq. GeoArabia, 15 (4), p.49-76.

Al-Naqib, K.M., 1967. Geology of the Arabian Peninsula, southern west Iraq. United States Geological survey, Professional Paper, No. 560-G, 54P.Al-Zainaldin, S., Glover, P.W.J. and Lorinczi, P., 2017. Synthetic Fractal Modelling of Heterogeneous and Anisotropic

Reservoirs for Use in Simulation Studies: Implications on Their Hydrocarbon Recovery Prediction. Transport in Porous Media, 116(1), p. 181-212.

Alsharhan, A. S., and Nairn, A. E. M., 1997, Sedimentary Basin and Petroleum Geology of the Middle East, Elsevier Science, 942 p.

Amthor, J. E., & Friedman, G. M. 1992. Early-to late-diagenetic dolomitization of platform carbonates; lower Ordovician Ellenburger Group, Permian Basin, west Texas. Journal of Sedimentary Research, 62(1), p.131-144.

Aqrawi, A.A., Goff, J.C. , Horbury , A.D. and Saddni, F. 2010. The petroleum geology of Iraq. Scientific Press Ltd, Beacon field, Bucks, 424 p.

Asquith, G., and Krygowski, D., 2004. Basic well log analysis. American Association of Petroleum Geologists, Tulsa, Oklahoma, 244 p.

Bjørlykke, K., 2010, Petroleum Geoscience: from sedimentary environments to rock physics, Springer-Verlag Berlin Heidelberg, 508p.

Chatton, M., 1997. The Wajnah Formation: a new name for a Cretaceous lithostratigraphic unit in Iraq. Iraqi geological journal, 30 (1), p. 4-6.

Childs, C., Walsh, J.J., Watterson, J., 1997. Complexity in fault zone structure and implications for fault seal prediction. In: Møller-Pedersen, P., Koestler, A.G. (Eds.), Hydrocarbon Seals: Importance for Exploration and Production. (Elsevier) Norwegian Petroleum Society Special Publication, 7, p. 61–72.

Choquette, P.W., and Pray, L.C., 1970. Geological Nomenclature and classification of porosity in sedimentary carbonates. American Association of Petroleum Geologists Bulletin, 54, p. 819-834.

Dickson, J.A.D., 1965. A modified staining technique for carbonates in thin section: Nature, 205, p.587-587.

Dunnington, H. V., 1958. Generation, Migration, Accumulation and Dissipation of Oil in Northern Iraq: Middle East, American Association of Petroleum Geologists, special volume, p. 1194-1251.

Ehrenberg, S.N. and Nadeau, P.H. 2005. Sandstone vs. carbonate petroleum reservoirs: A global perspective on porosity-depth and porosity permeability relationships. AAPG Bulletin, 89 (4), p. 435–445.

Ehrenberg, S.N. 2006. Porosity Destruction in Carbonate Platforms: Journal of Petroleum Geology, 29, p. 41-52.

Ehrenberg, S.N., Aqrawi, A.A. and Nadeau, P.H., 2008. An overview of reservoir quality in producing Cretaceous strata of the Middle East. Petroleum Geoscience, 14 (4), p.307-318.

Erdman, N. and Bell, D.C., 2015. Scanning Electron and Ion Microscopy of Nanostructures. In Nanocharacterisation, Royal Society of Chemistry, p. 300-350.

Esrafili-Dizaji, B. and Rahimpour-Bonab, H., 2009. Effects of depositional and diagenetic characteristics on carbonate reservoir quality: a case study from the South Pars gas field in the Persian Gulf. Petroleum Geoscience, 15 (4), p.325-344.

Flugel, E., 2010. Microfacies of carbonate rocks. Verlag Berlin Heidelberg, 984 p.

Folk, R.L., 1962. Spectral subdivision of limestone types. p.62-84.

Fouad, S. F. A., 2015. Tectonic map of Iraq, scale 1: 1000 000, 3rd edition, Iraqi Bulletin of Geology and Mining, Papers of the Scientific Geological Conference, 11, p. 1-7.

Friedman, G.M., 1965: Terminology of crystallization textures and fabrics in sedimentary rocks. J. Sedimentary petrology 35, p.643-655.

Géraud, Y., Diraison, M. and Orellana, N., 2006. Fault zone geometry of a mature active normal fault: a potential high permeability channel (Pirgaki fault, Corinth rift, Greece). Tectonophysics, 426(1), p.61-76.

Giesche, H., 2006. Mercury porosimetery: a general (practical) overview. Part. Part. Syst. Charact. 23, p. 9-19.

Glover, P.W.J., 2010. A generalized Archie's law for n phases. Geophysics, 75 (6), p.247-265.Glover, P.W.J., 2015. Geophysical properties of the near surface Earth: Electrical properties. Treatise on Geophysics, 11, p.89-137.

Glover, P.W.J., Zadjali, I. and Frew, K. 2006.Permeability prediction from MICP and NMR data using an electro-kinetic approach, Geophysics, 71, F49.

Glover, P.W.J. and Walker, E., 2009. Grain-size to effective pore-size transformation derived from electrokinetic theory. Geophysics, 74(1), p. E17-E29.

Glover, P.W.J. and Déry, N., 2010. Streaming potential coupling coefficient of quartz glass bead packs: Dependence on grain diameter, pore size, and pore throat radius. Geophysics, 75(6), p. F225-F241.Glover, P.W.J., Lorinczi, P., Al-Zainaldin, S., Al-Ramadan, H., Daniel, G. and SINAN, S., 2018. Advanced fractal modelling of heterogeneous and anisotropic reservoirs, SPWLA 59th Annual Logging Symposium 2018.

Glover, P.W.J., 2015. Geophysical properties of the near surface Earth: Electrical properties. p. 89-137.

Glover, P.W., Lorinczi, P., Al-Zainaldin, S., Al-Ramadan, H., Daniel, G. and Sinan, S., 2018, June. Advanced Fractal Modelling of Heterogeneous and Anisotropic Reservoirs. In SPWLA 59th Annual Logging Symposium. Society of Petrophysicists and Well-Log Analysts.

Gluyas, J. and R. Swarbrick, 2004. Petroleum Geoscience (Xth edn.). Blackwell Science Ltd, 349 p.

Hanshaw, B.B., Back, W. and Deike, R.G., 1971. A geochemical hypothesis for dolomitization by ground water. Economic Geology, 66(5), p.710-724.

Haines T.J., Michie, E.A.H., Neilson, J.E., and Healy, D. 2016. Permeability evolution across carbonate hosted normal fault zones, Marine and Petroleum Geology, 72, p. 62-82.

Harris, P.M. 2010. Delineating and quantifying depositional facies patterns in carbonate reservoirs: Insight from modern analogues, AAPG Bulletin, 94, (1), p.61–86.

Hart, E. and J.T.C. Hay, 1974, Structure of Ain Zalah Field, Northern Iraq. AAPG Bulletin, 58(6), p.973-981.

Hollis, C., Vahrenkamp, V., Tull, S., Mookerjee, A., Taberner, C. and Huang, Y., 2010. Pore system characterisation in heterogeneous carbonates: An alternative approach to widely-used rock-typing methodologies. Marine and Petroleum Geology, 27, p. 772-793.

Hollis, C., Bastesen, E., Boyce, A., Corlett, H., Gawthorpe, R., Hirani, J., Rotevatn, A. and Whitaker, F., 2017. Fault-controlled dolomitization in a rift basin. Geology, 45 (3), p.219-222.

Hsü, K.J. and Siegenthaler, C., 1969. Preliminary experiments on hydrodynamic movement induced by evaporation and their bearing on the dolomite problem. Sedimentology, 12, p.11-25.Hussein, D., Collier, R., Lawrence, J.A., Rashid, F., Glover, P.W.J., Lorinczi, P. and Baban, D.H., 2017. Stratigraphic correlation and paleoenvironmental analysis of the hydrocarbon-bearing Early Miocene Euphrates and Jeribe formations in the Zagros folded-thrust belt. Arabian Journal of Geosciences, 10(24).

Hussein, D., Collier, R., Lawrence, J.A., Rashid, F., Glover, P.W.J., Lorinczi, P. and Baban, D.H., 2017. Stratigraphic correlation and paleoenvironmental analysis of the hydrocarbon-bearing Early Miocene Euphrates and Jeribe formations in the Zagros folded-thrust belt. Arabian Journal of Geosciences, 10(24), p.543.

Illing, L.V., Wells, A.J., Taylor, J.C.M., 1965. Penecontemporaneous dolomite in the Persian Gulf. In: Pray, L.C., Murray, R.C. (eds.), Dolomitisation and limestone diagenesis. Society of Econologists, Palaeontologists and Mineralogists, Special Publication, 13, p. 89-111.

Jannot, Y., Lasseux, D., Vizé, G. and Hamon, G. 2007. A detailed analysis of permeability and Klinkenberg coefficient estimation from unsteady-state pulse-decay or draw-down experiments. Paper no. SCA2007-08.

Jassim, S.Z., and Goff J. C., 2006, Phanerozoic development of the Northern Arabian Plate. In: Jassim, S.Z. and Goff, J.C. (eds) Geology of Iraq. Dolin, Prague and Moravian Museum, Brno. p. 30-44.

Jassim, S.Z. and Buday, T., 2006. Late Tithonian-Early Turonian Megasequence AP8. In: Jassim, S.Z. and Goff, J.C. (eds) Geology of Iraq. Dolin, Prague and Moravian Museum, Brno. p. 124-140.

Jassim, S. Z., Buday, T., Cicha, I., and Prouza, V., 2006. Late Permian-Liassic Megasequence AP6. In: Jassim, S.Z. and Goff, J.C. (eds) Geology of Iraq. Dolin, Prague and Moravian Museum, Brno. p. 104-116.

Jennings, J.B. 1987. Capillary Pressure Techniques: Application to Exploration and Development Geology. AAPG Bulletin, 71, p.1196-1209.

Jones, S.C. 1997. A Technique for Faster Pulse-Decay Permeability Measurements in Tight Rocks. Society of Petroleum Engineers, SPE-28450-PA.

Kaddouri, N., 1982, Tel Hajar: A new Cenomanian-Lower Turonian stratigraphic unit from North-west Iraq, Cretaceous Research, 3, p. 391-395.

Kaldi, J., & Gidman, J. 1982. Early diagenetic dolomite cements; examples from the Permian Lower Magnesian Limestone of England and the Pleistocene carbonates of the Bahamas. Journal of Sedimentary Research, 52 (4), p.1073-1085.

Katz, A. J. and Thompson, A. H. 1987. Prediction of rock electrical conductivity from mercury injection measurements, Geophysical research, 92, p.599-607.

Keith, M.L. and Weber, J.N., 1964. Carbon and oxygen isotopic composition of selected limestones and fossils. Geochimica et Cosmochimica Acta, 28(10-11), pp.1787-1816.

Klinkenberg, L.J., 1941. The permeability of porous media to liquids and gases. Drill. Prod. Pract. 200e213.

Kopaska-Merkel, D.C. and Amthor, J.E. 1988. Very high pressure mercury porosimetry as a tool in reservoir characterization, Carbonate Evaporite, 3, p.53–63.

Kyser, T. K., James, N. P., & Bone, Y. 2002. Shallow burial dolomitization and dedolomitization of Cenozoic cool-water limestones, southern Australia: geochemistry and origin. *Journal of Sedimentary Research*, *72*(1), p.146-157.

Larsen, B., Grunnaleite, I. and Gudmundsson, A. 2010. How fracture systems affect permeability development in shallow-water carbonate rocks: an example from the Gargano Peninsula. Italy. J. Struct. Geol. 32, 1212e1230.

Lonoy, A., 2006. Making sense of carbonate pore systems. American Association of Petroleum Geologists, 90, p. 1381-1405.

Lucia, F.J., 1983. Petrophysical parameters estimated from visual description of carbonate rocks: a field classification of carbonate pore space. Journal of Petroleum Technology, v. 35, p. 626-637.

Lucia, F.J., 1995. Rock-fabrics/ Petrophysical classification of carbonate pore space for reservoir characterization. American Association of Petroleum Geologists, 79, p. 1275-1300.

Lucia, F.J., 1999. Carbonate Reservoir Characterization: Springer-Verlag, Berlin.

Lucia, F.J., 2004. Origin and petrophysics of dolostone pore space. Geological Society, London, Special Publications, 235(1), p.141-155.

Lucia, F.J. 2007 .Carbonate Reservoir Characterization: an Integrated Approach, (second edition) Springer .

Luo, P., and Marchel, G., 1995. Pore size and pore throat types in a heterogeneous dolostone reservoir; Devonian Grosmon Formation, Western Canada basin. American Association of Petroleum Geologists Bulletin, 79, p. 1698-1720.

Machel, H.G., 2004. Concepts and models of dolomitisation: a critical reappraisal. In: Braithwaite, C.J., Rizzi, G. and Darke, G., 2004. The geometry and petrogenesis of dolomite hydrocarbon reservoirs. Geological Society, London, Special Publications, 235(1), p. 7-63.

Machel, H.G. and Mountjoy, E.W., 1986. Chemistry and environments of dolomitization—a reappraisal. *Earth-Science Reviews*, *23*(3), p.175-222.

McPhee, C., Reed, J., Zubizarreta ,I .2015. Core Analysis : A best practice guide , first edition, 830p.

Moore, C. H., 2001. Carbonate reservoirs, porosity evaluation and diagenesis in a stratigraphic sequence framework, Developments in sedimentology, Netherland, 55, 444 p.

Morrow, D.W., 1982. Diagenesis 2. Dolomite - Part 2 Dolomitisation models and Ancient dolostones. Geoscience Canada, 9 (2), p. 95-107.

Morrow, D.W., Cumming, G.L. and Keopnick, R.B., 1986. Manetoe Facies- A gas-bearing megacrystalline, Devonian dolomite, Yukon and Northwest Territories, Canada. AAPG Bulletin, 70 (6), p.702-720.

North, F.K., 1985. Petroleum Geology (Xth edn.). George Allen and Unwin Ltd. Sydney, Australia, 607 p.

Palermo, D., Aigner, T., Nardon, S., and Blendinger, W. 2010. Three-dimensional facies modelling of carbonate sand bodies: outcrop analogue study in an epicontinental basin (Triassic, southwest Germany), AAPG Bulletin, 94, p.475–512.

Randazzo, A.F. and Zachos, L.G., 1984. Classification and description of dolomitic fabrics of rocks from the Floridan aquifer, USA. Sedimentary geology, 37 (3), p.151-162.

Rashid, F., Glover, P.W.J., Lorinczi, P., Collier, R. and Lawrence, J. 2015a. Porosity and permeability of tight carbonate reservoir rocks in the north of Iraq. Journal of Petroleum Science and Engineering, 133, p.147-161.

Rashid, F., Glover, P.W.J., Lorinczi, P., Hussein, D., Collier, C and Lawrence J. 2015b. Permeability prediction in tight carbonate rocks using capillary pressure measurements, Marine and Petroleum Geology, 68, 536-550.Rashid, F., Glover, P.W.J., Lorinczi, P., Hussein, D. and Lawrence, J.A., 2017. Microstructural controls on reservoir quality in tight oil carbonate reservoir rocks. Journal of Petroleum Science and Engineering, 156, p. 814-826.

Rashid, F., Glover, P.W.J., Lorinczi, P., Hussein, D. and Lawrence, J.A., 2017. Microstructural controls on reservoir quality in tight oil carbonate reservoir rocks. Journal of Petroleum Science and Engineering, 156, p.814-826.

Ren, Y., Zhong, D., Gao, C., Yang, Q., Xie, R., Jia, L., Jiang, Y. and Zhong, N., 2017. Dolomite geochemistry of the Cambrian Longwangmiao Formation, Eastern Sichuan Basin: implication for dolomitization and reservoir prediction. Petroleum Research, 2(1), p.64-76.

Ronchi, P., Giulio, A. D, Ceriani, A. and Scotti, P. 2010. Contrasting fluid events giving rise to apparently similar diagenetic products; late-stage dolomite cements from the Southern

Alps and central Apennines, Italy, Geological Society of London, Special Publications, 329, p.397–413.

Rushing, J.A., Newsham, K.E., Lasswel,P.M. l, Cox, J.C., and Blasingame, T.A.2004. Klinkenberg-Corrected Permeability Measurements in Tight Gas Sands: Steady-State.Versus Unsteady-State Techniques. SPE 89867.

Sadeq, Q., M., and Yusoff, W. I. B. W., 2015. Porosity and Permeability Analysis from Well Logs and Core in Fracture, Vuggy and Intercrystalline Carbonate Reservoirs. Journal of Aquaculture, v. 6, Issue 10.1000371, p.1-5.

Sahar, A. A., 1987. Dolomitisation of Upper Qamchuqa Formation Northern Iraq. Unpublished, M.Sc thesis University of Baghdad.182p.

Spain, D. R. 1992. Petrophysical evaluation of a slope fan/ basin floor fan complex: cherry canyon formation, Ward County, Texas. AAOG Bulletin, 76, p.805-827.

Schmoker, J. W., and R. B. Halley, 1982. Carbonate porosity versus depth: a predictable relation for south Florida: AAPG Bulletin, v. 66, p. 2561-2570.

Scholle, P., A., and D. Ulmer-Scholle, S., 2003. A colour guide to the petrography of carbonate rocks: grains, textures, porosity, diagenesis. American Association of Petroleum Geologists Bulletin, 77, Tulsa, Oklahoma, U.S.A.

Sharland P .R ., Archer R ., Casey D.M., Davies R .B. , Hall S .H., Heward A.P ., Horbury A.D. and Simmons M.D., 2001. The Chrono-Sequence Stratigraphy of the Arabian Plate. GeoArabia Special Publication 2, Gulf petrolink, Bahrain, 371p.

Tavakoli, V., Rahimpour-Bonab, H. and Esrafili-Dizaji, B., 2011. Diagenetic controlled reservoir quality of south Pars gas field, an integrated approach. Comptes Rendus Geoscience, 343, p. 55- 71.

Tiab, D., and E.C. Donaldson, 2012. Petrophysics: Theory and practice of measuring reservoir rock and fluid transport properties 3rd edition. Elsevier, 950 p.

Tucker, M. E., 1991. Sedimentary Petrology, an introduction to the origin of Verlag, Berlin Heidelberg New York, 260p.

Ward, W. C., & Halley, R. B. (1985). Dolomitization in a mixing zone of near-seawater composition, late Pleistocene, northeastern Yucatan Peninsula. Journal of Sedimentary Research, 55 (3), p. 407-420.

Warren, J., 2000. Dolomite: occurrence, evolution and economic important associations. Earth-Science Reviews, 52, p.1-81.

Washburn, E.W. 1921. The Dynamics of Capillary Flow, Physical Review, 17, 273-283.

Wright, V. P. 1992. A revised classification of limestones. Sedimentary geology, 76, p.177-185.

Zhang, M., Takahashi, M., Morin, R. H. and Esaki, T. 2000. Evaluation and Application of the Transient-Pulse Technique for Determining the Hydraulic Properties of Low-Permeability Rocks – Part 1: Theoretical Evaluation. American Society for Testing and Materials : Geotechnical Testing Journal, p.83-90.

Zhang, L., Jiao, Y., Rong, H., Li, R. and Wang, R., 2017. Origins and Geochemistry of Oolitic Dolomite of the Feixianguan Formation from the Yudongzi Outcrop, Northwest Sichuan Basin, China. Minerals, 7(120), p.1-21.

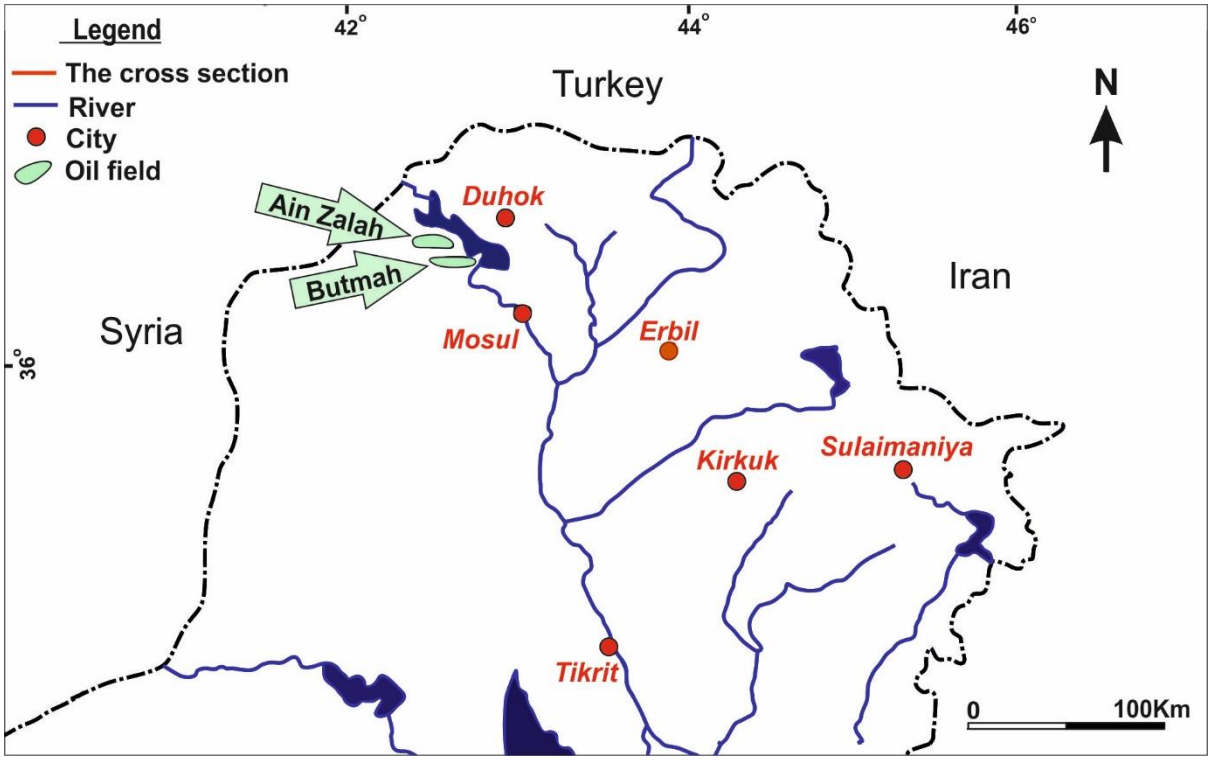

Figure 1. The location of the Butmah and Ain Zalah oilfields in north-western Iraq.

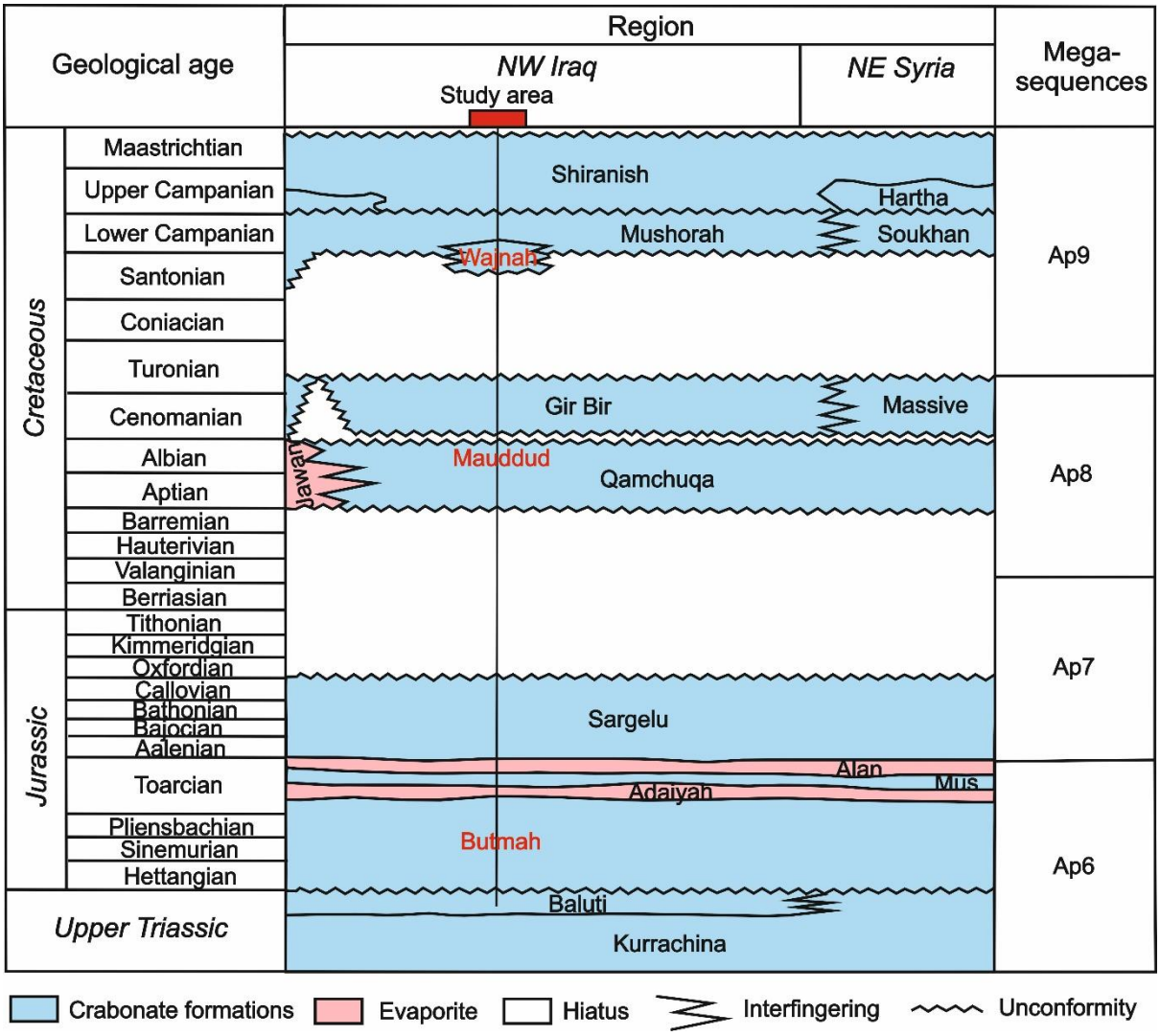

Figure 2. Stratigraphic correlation section of the studied formations in north-western Iraq and north-eastern Syria. Modified after (Al-Naquib, 1967; Kaddouri, 1982).

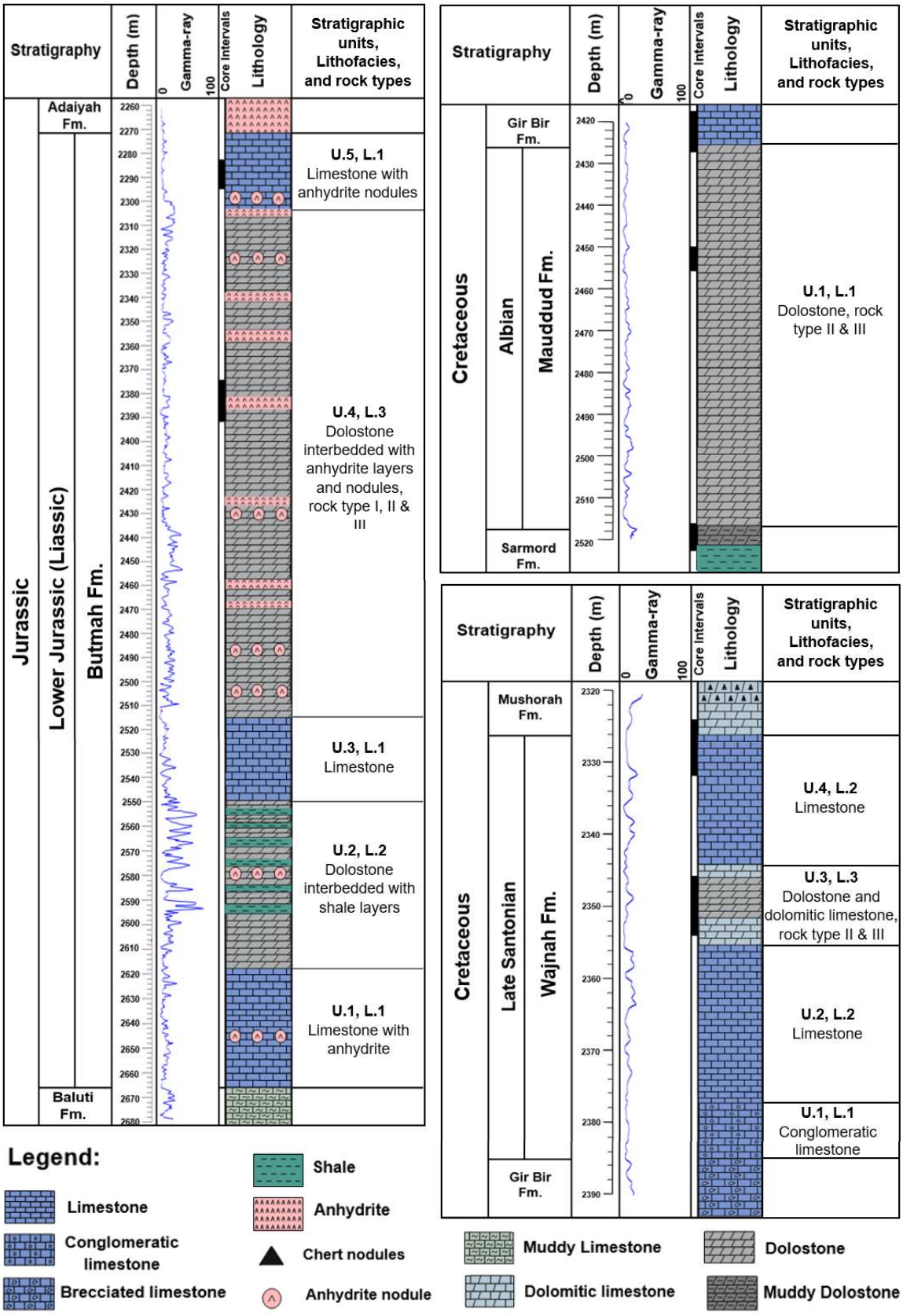

Figure 3. Stratigraphic units of the Butmah Formation in well Bm-15 (left), the Mauddud (top right) and Wajnah (bottom right) formations in well Az-16. Where U= Stratigraphic unit, L= Lithofacies.

Dolomitization Model	Source of Mg^{2+}	Delivery Mechanism	Hydrological Model	Predicted Dolomite Patterns
A. Reflux Dolomitization	seawater	storm recharge, evaporative pumping density-driven flow	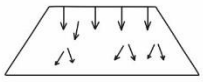	
B. Mixing Zone (Dorag) Dolomitization	seawater	tidal pumping	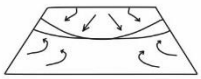	
C1. Seawater Dolomitization	normal seawater	slope convection ($K_V > K_H$)	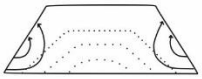	
C2. Seawater Dolomitization	normal seawater	slope convection ($K_H > K_V$)	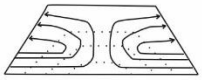	
D1. Burial Dolomitization (local scale)	basinal shales	compaction-driven flow	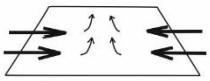	
D2. Burial Dolomitization (regional scale)	various subsurface fluids	tectonic expulsion topography-driven flow	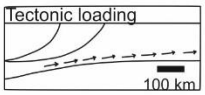	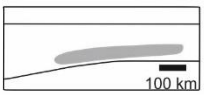
D3. Burial Dolomitization (regional scale)	various subsurface fluids	thermo-density convection	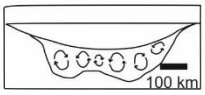	
D4. Burial Dolomitization (local and regional scales)	various subsurface fluids	tectonic reactivation of faults (seismic pumping)	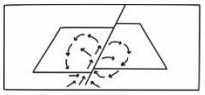	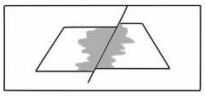

Figure 4. Dolomitisation models for a carbonate platform (modified and redrawn after Machel, 2004).

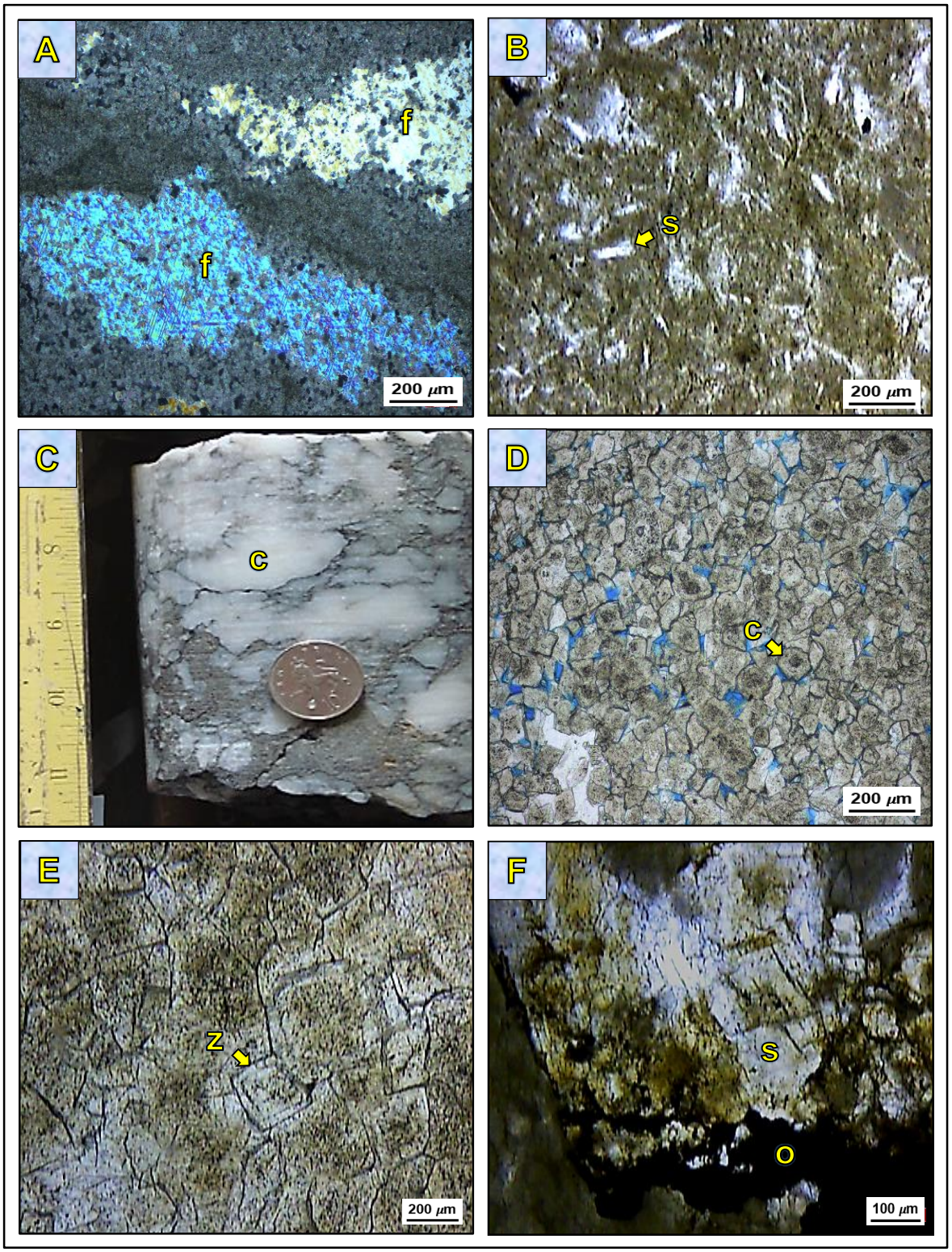

Figure 5. Experimental petrogtaphic evidence of diagenetic processes. A: Fenestral pores (F) occluded by anhydrite cement as early cementation in the Butmah Fm., Bm-15, (2488 m). B: Sparse anhydrite crystals (s) within fine crystalline dolomite in the Butmah Fm., Bm-15 (2422 m). C: Compressed chicken-wire texture (c) caused by compaction, Butmah Fm, Bm-15, (2379 m). D: Cloudy dolomite centres (c) surrounded by a clear limpid rim, Mauddud Fm., Az-16, (2446 m). E: Zoned coarse dolomite crystals (z) as late dolomitisation features in the Mauddud Fm., Az-16, (2472 m). F: Saddle dolomite (s) as a late dolomitisation feature associated with stylolite and oil shows (o), Mauddud Fm., Az-16, (2486 m).

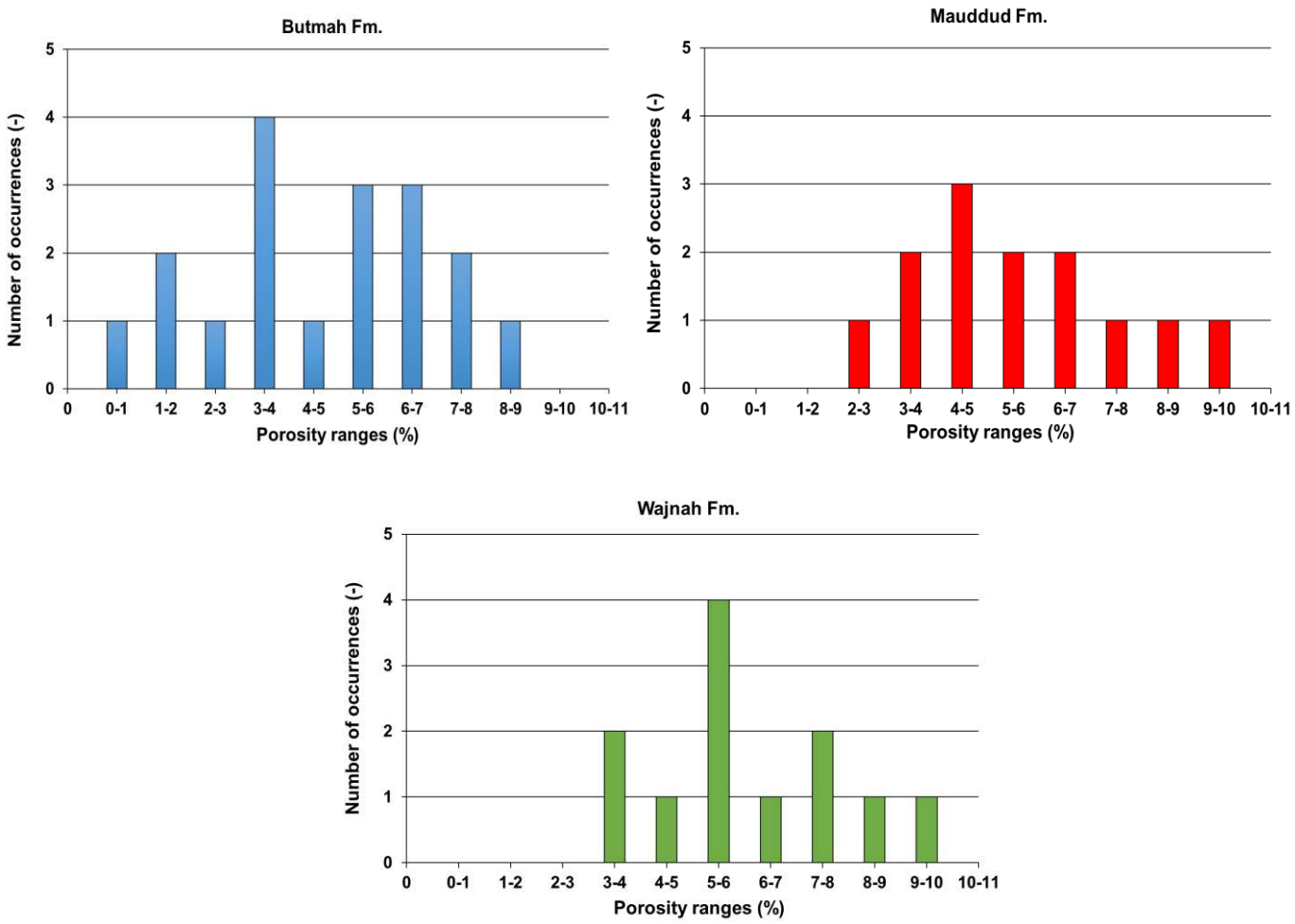

Figure 6. Histograms of the effective porosity of the Butmah Formation at well Bm-15, the Mauddud Formation and the Wajnah Formation at well Az-29.

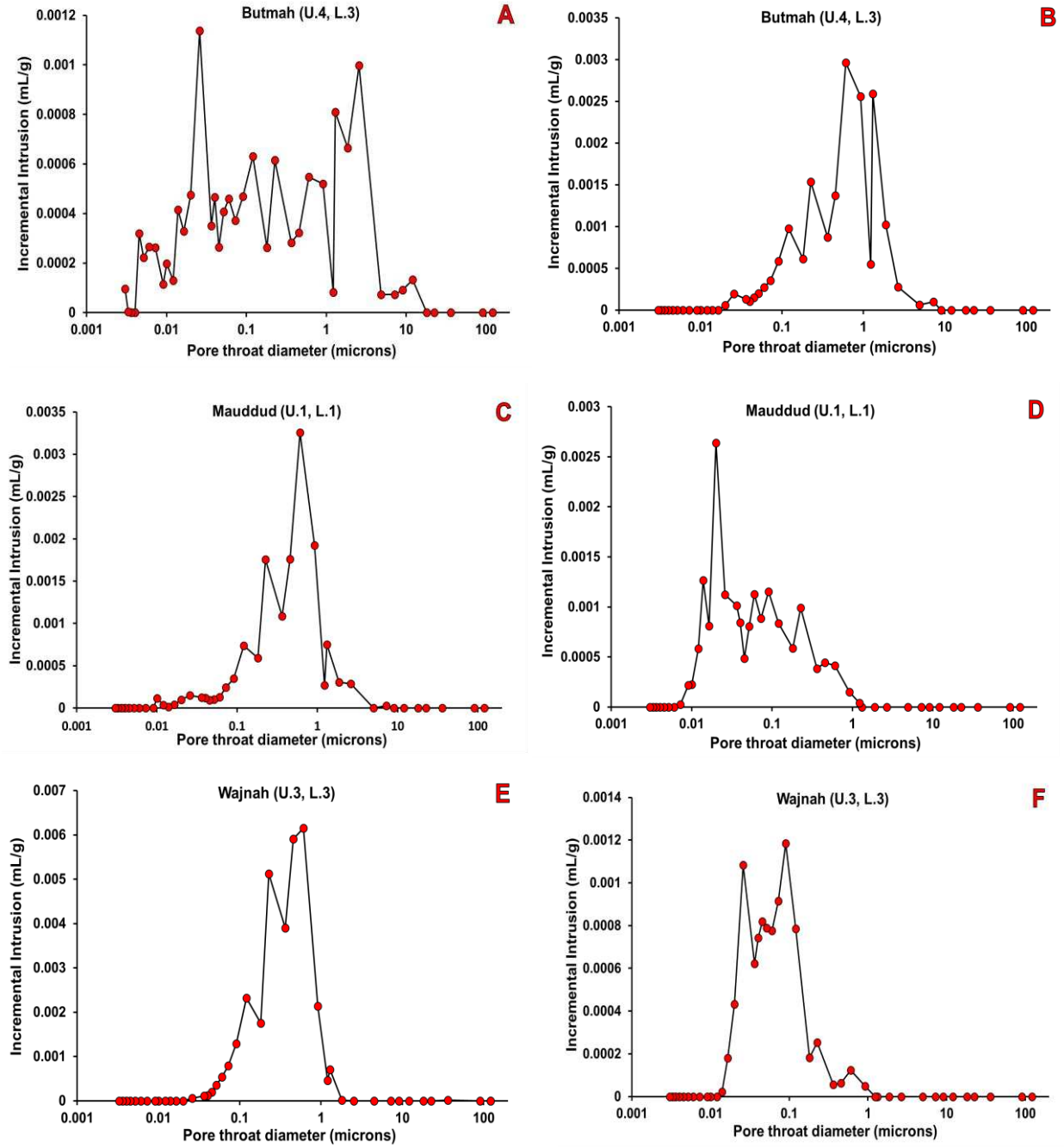

Figure 7. Pore throat distributions for six samples subjected to MICP measurements. Top row; two samples from the Butmah Formation, middle row; two from the Mauddud Formation, and bottom row; two samples from the Wajnah Formation.

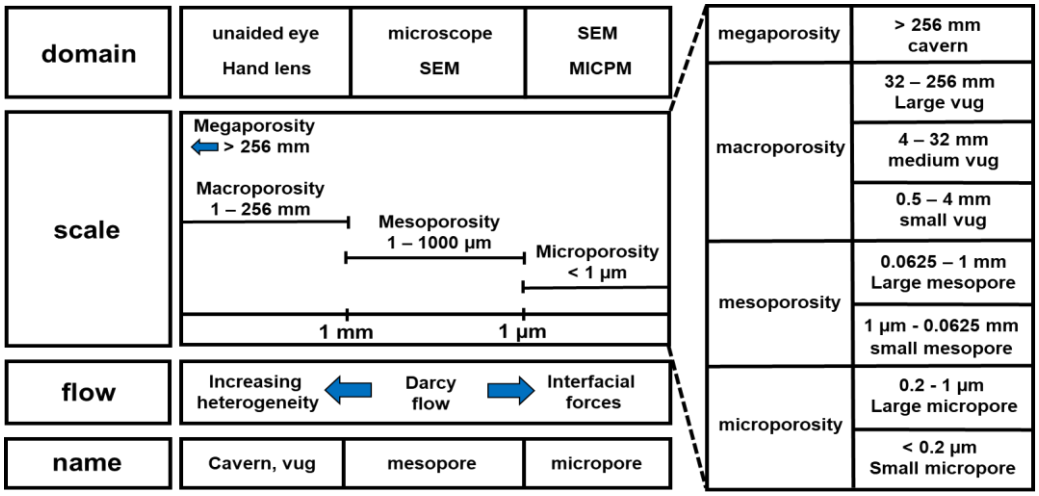

Figure 8. The pore size classification for carbonate rock. Luo and Machel, (1995).

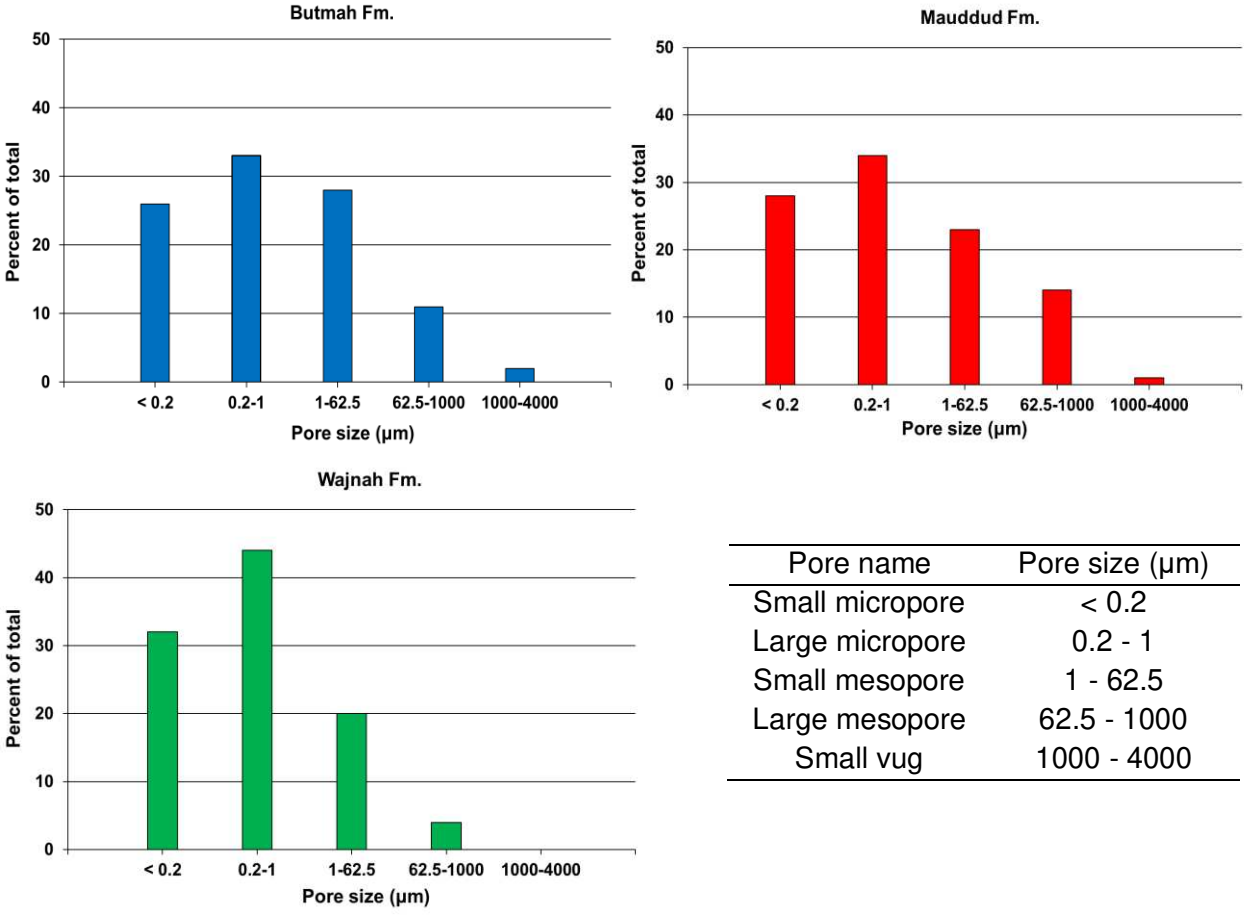

Pore name	Pore size (µm)
Small micropore	< 0.2
Large micropore	0.2 - 1
Small mesopore	1 - 62.5
Large mesopore	62.5 - 1000
Small vug	1000 - 4000

Figure 9. Histograms of pore size distribution within the Butmah, Mauddud, and Wajnah formations using pore size bins defined by the Luo and Machel, (1995) classification.

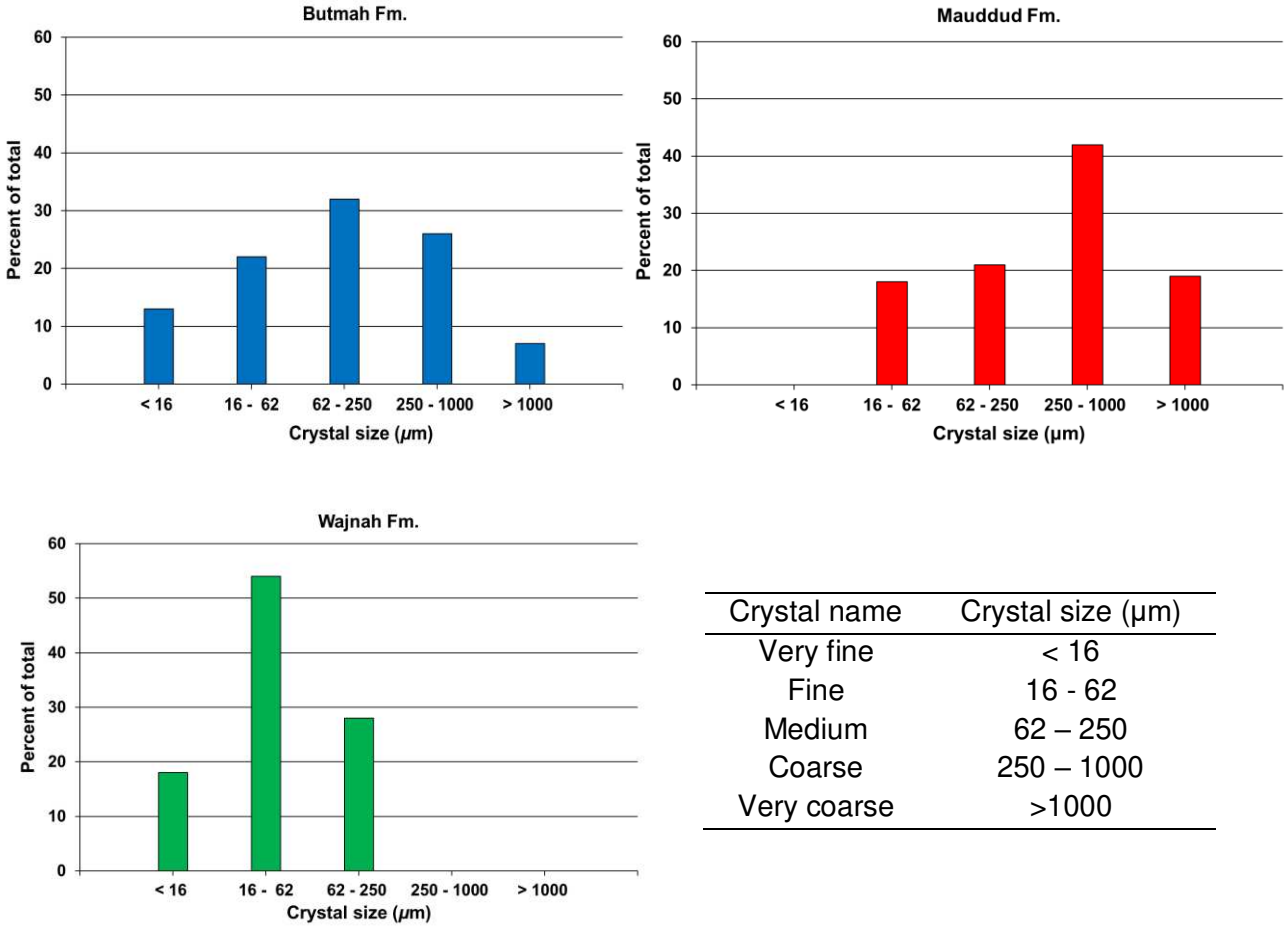

Crystal name	Crystal size (μm)
Very fine	< 16
Fine	16 - 62
Medium	62 – 250
Coarse	250 – 1000
Very coarse	>1000

Figure 10. Histograms of crystal size distribution within the Butmah, Mauddud, and Wajnah formations using crystal size bins defined in this work.

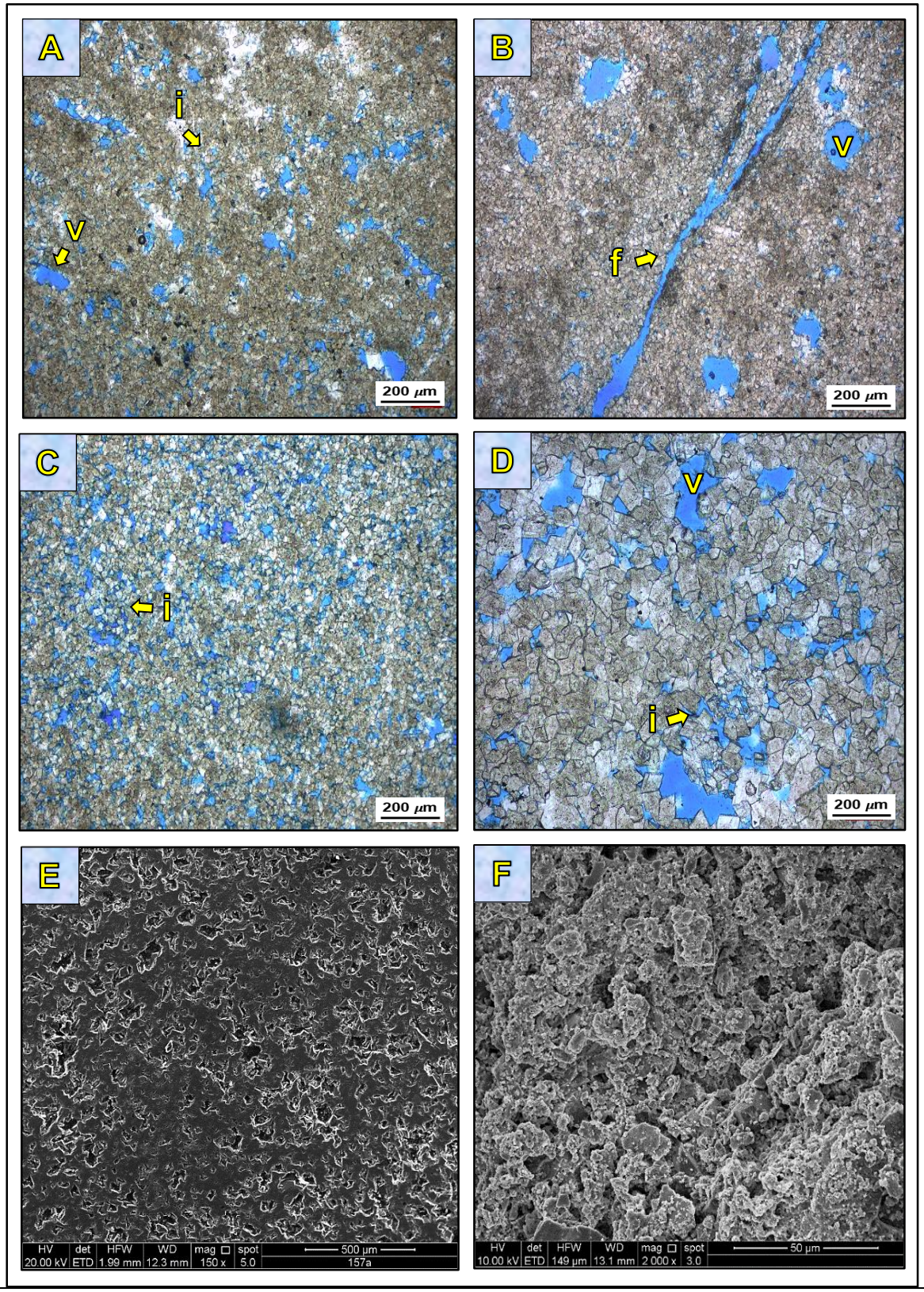

Figure 11. A: Intercrystalline porosity (i) and vuggy porosity (v), Butmah Fm., Bm-15, U.4 (2450 m). B: Vuggy (v) and fractures (f) porosity, Butmah Fm., Bm-15, U.4 (2450 m). C: intercrystalline porosity (i), Butmah Fm., Bm-15, U.2 (2597 m). D: vuggy (v) and intercrystalline (i) porosity of medium dolomite crystals, Mauddud Fm. Az-16, U.1, (2452 m). E and F: are SEM images showing pore shape and size in 2D and 3D, respectively, for a sample from the Butmah Fm., Bm-15, U.4 (2388 m).

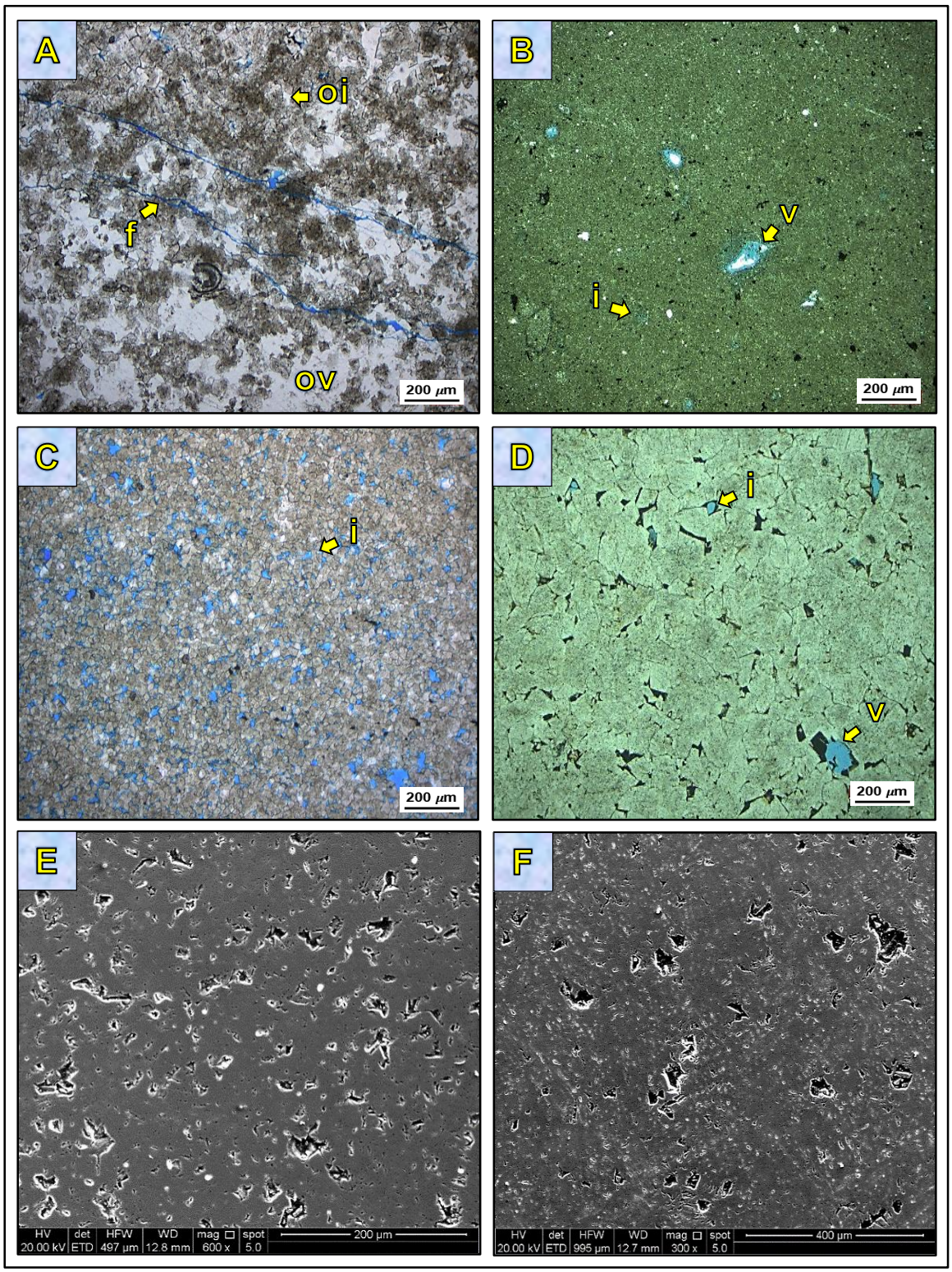

Figure 12. A: Fracture porosity (f) and anhydrite cement occluding intercrystalline (oi) and vuggy pores (ov), Butmah Fm., Bm-15, U.4 (2450 m). B: very fine crystalline dolomite with some vugs (v) and intercrystalline (i) pores, Wajnah Fm., Az-16, U.3 (2349 m). C: Intercrystalline porosity (i) of fine crystalline dolomite, Wajnah Fm., Az-16, U.3 (2351 m). D: intercrystalline (i) and vuggy (v) porosity of medium dolomite crystals, Mauddud Fm., Az-16, U.1, (2484 m). E: intercrystalline porosity, Butmah Fm., Bm-15, U.2 (2597 m). F: SEM images showing pore shape and size in 2D in the Wajnah Fm., Az-16, U.3 (2350 m) and Mauddud Fm. Az-16, U.1 (2453 m), respectively.

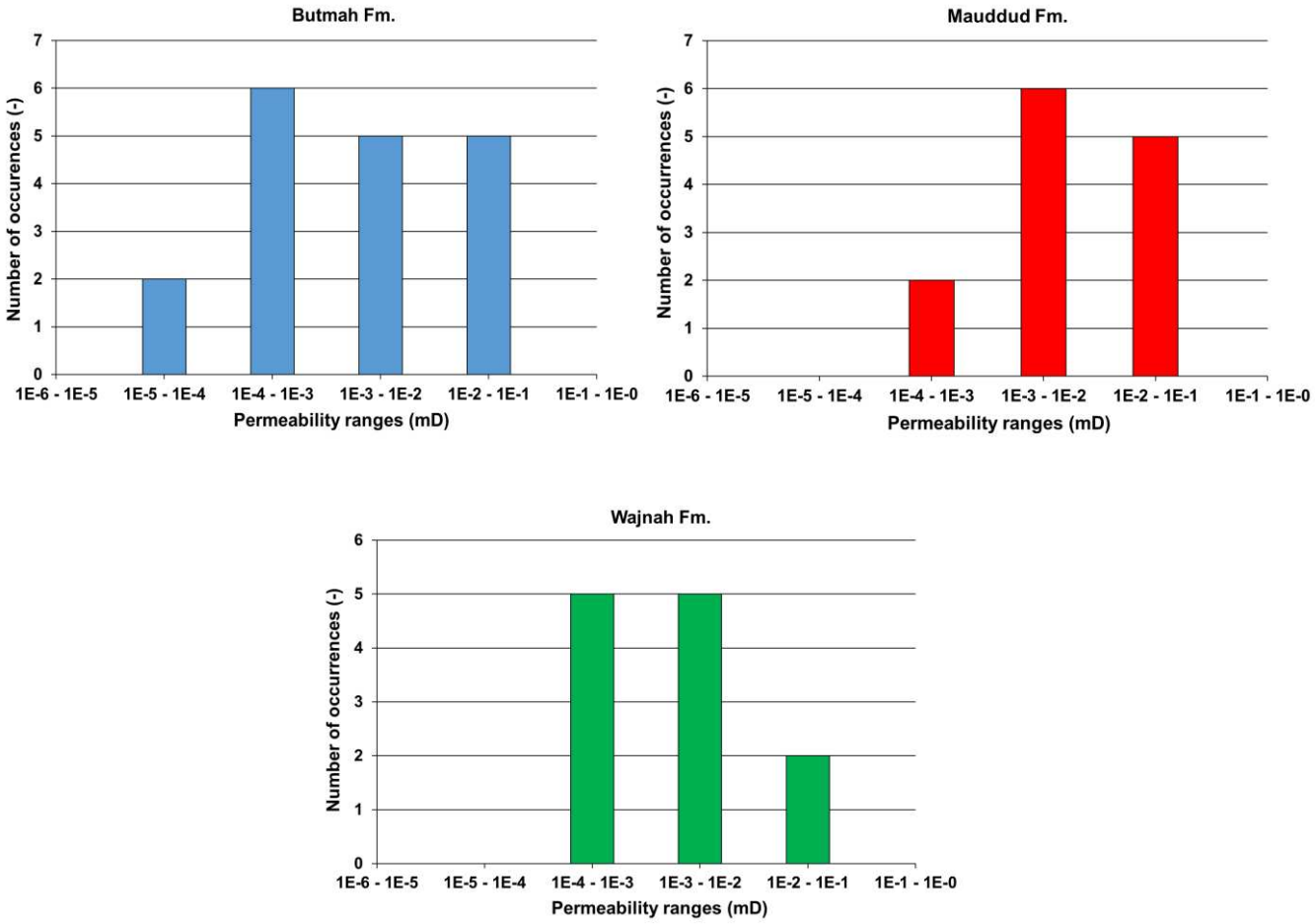

Figure 13. Permeability histograms and pie charts of the Butmah Formation at well Bm-15, the Mauddud Formation and Wajnah Formation at well Az-29.

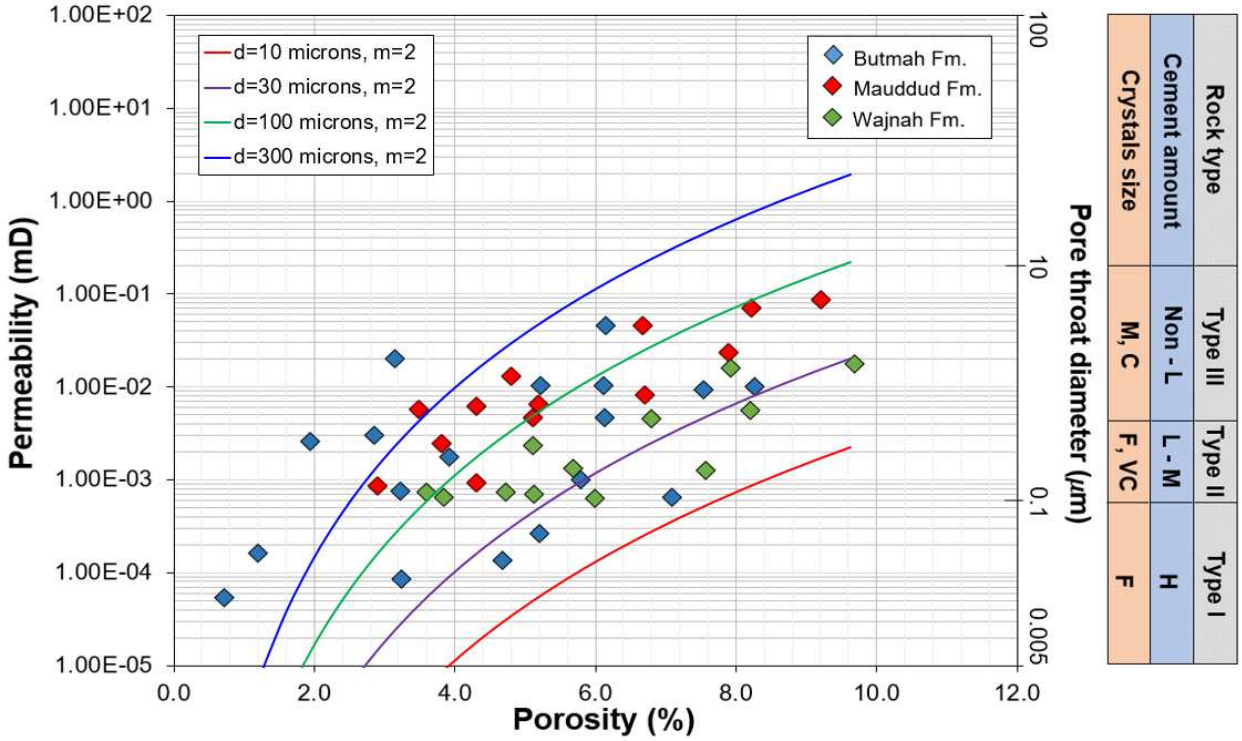

Figure 14. Porosity - permeability relationships of the Butmah, Mauddud and Wajnah formations, showing the identified rock types according to the relationship and the distribution pore throat diameter, crystal size, and amount of cement. In the blue cement amount bar L = low, M= moderate, H= high. In the orange crystal size bar; F= fine crystals, M= medium crystals, C= coarse crystals, and VC= very coarse crystals.

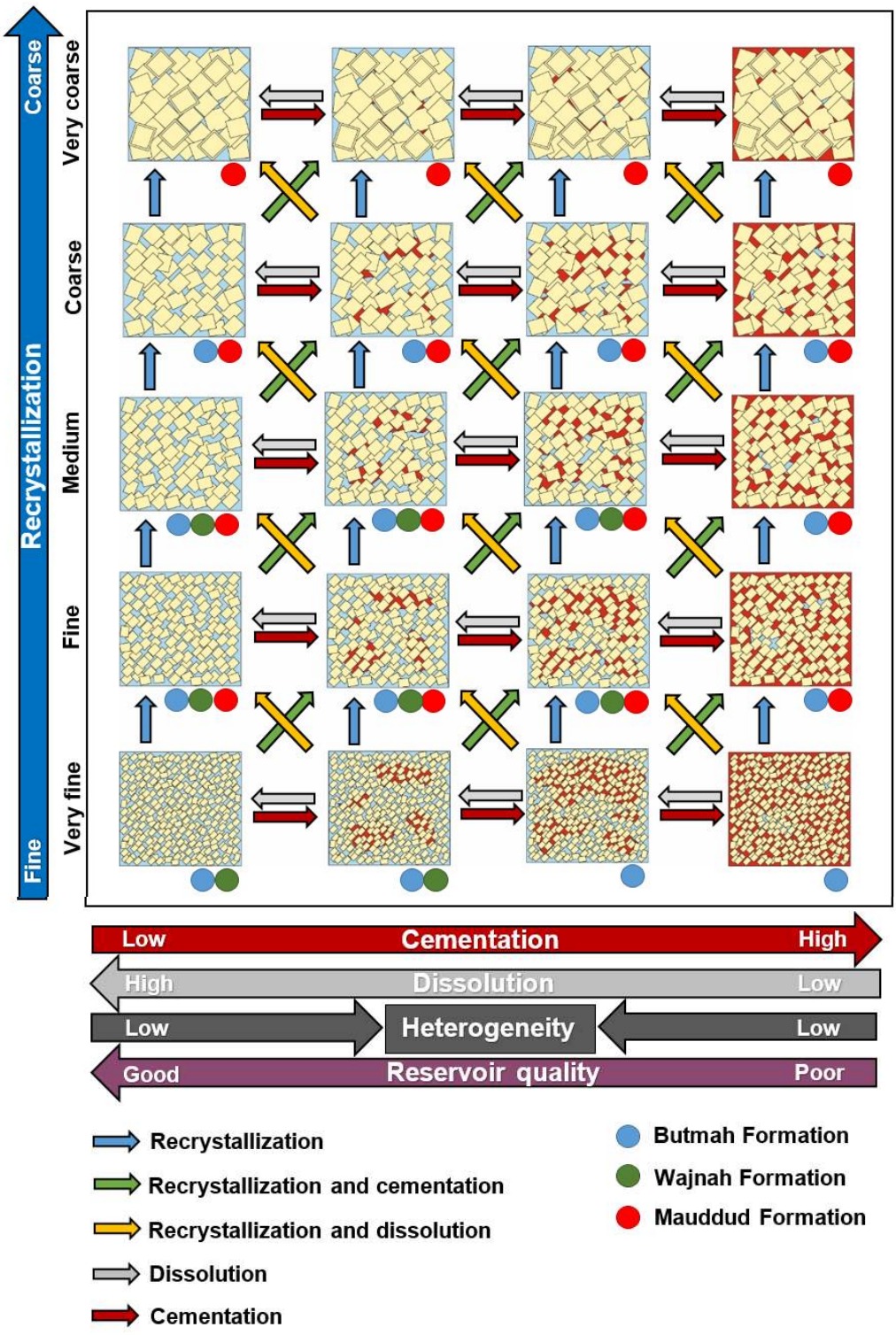

Figure 15. Recrystallisation versus dissolution and cementation effects on the reservoir properties and heterogeneity of the studied formation samples.

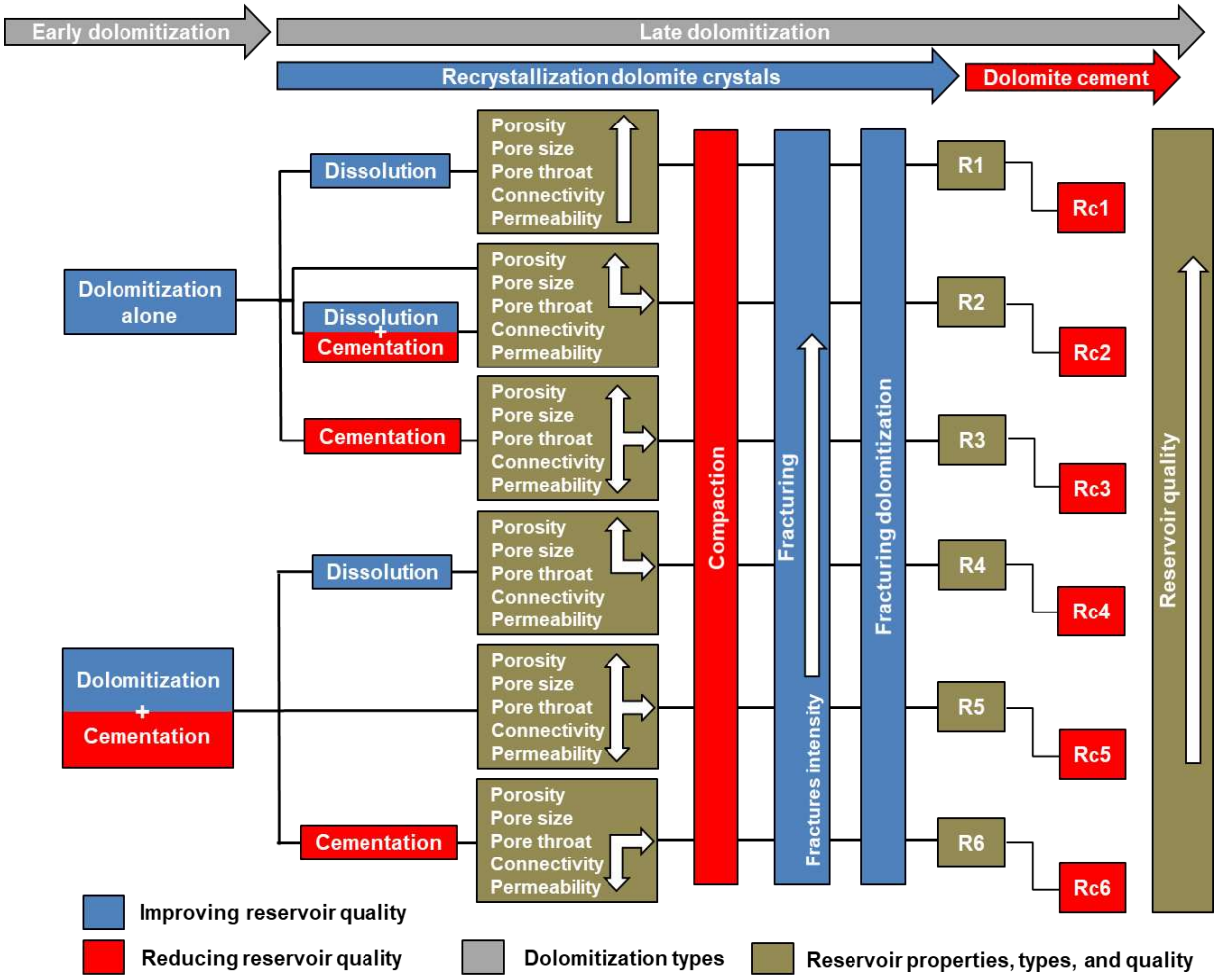

Figure 16. Flow chart shows the process-driven outcome reservoir types (PDRTs) for dolomitized rock.